THE PENNSYLVANIA STATE UNIVERSITY
SCHREYER HONORS COLLEGE

DEPARTMENT OF CHEMISTRY

IMPACTS OF SURFACE LIGAND COVERAGE ON THE ELECTRONIC PROPERTIES OF THIOL-PROTECTED GOLD NANOPARTICLES

JONATHAN HAIDET
SPRING 2024

A thesis
submitted in partial fulfillment
of the requirements
for baccalaureate degrees
in Chemistry
with honors in Inorganic Chemistry

Reviewed and approved* by the following:

Benjamin J. Lear
Professor of Chemistry
Thesis Supervisor

David D. Boehr
Professor of Chemistry
Associate Head for Undergraduate Education in Chemistry
Honors Adviser

Christine Keating
Distinguished Professor of Chemistry
Faculty Reader

*Signatures are on file in the Schreyer Honors College.

Abstract

Metallic nanoparticle research is a branch of inorganic chemistry with potential in optics, electrochemistry, catalysis, biochemistry, and more. Within the field of nanoparticle chemistry, thiol-protected gold nanoparticles (AuNPs) are a widely utilized system in chemical research due to their stability and ease of synthesis among other considerations. Despite their prevalence in chemical literature, our understanding of how surface chemistry impacts the behavior of thiol-protected AuNPs remains incomplete. Similarly to how molecular inorganic chemists are afforded control over the electronic properties of metal complexes through ligand binding, it is anticipated that surface chemistry can likewise alter the electronic properties of AuNPs, thus allowing for increasingly targeted applications of these systems. In a prior publication by our group, we established that ligand identity influences electronic properties; however, the relationship to surface ligand density has yet to be explored. Herein we present a synthetic method by which the surface ligand density can be modified while retaining constant morphological characteristics, including size and shape. Subsequently, we delve into the examination of the electronic properties of these nanoparticles using Evans' Method NMR to probe the density of electronic states near the fermi energy. This investigation aims to elucidate how alterations in surface ligand density impact the electronics of AuNPs, ultimately affording nanoparticle chemists similar electronic control to that enjoyed by molecular inorganic chemists.

Table of Contents

List of Figures

List of Abbreviations

NPs	Nanoparticles
AuNPs	Gold Nanoparticles
PdNPs	Palladium Nanoparticles
MOs	Molecular Orbitals
HOMO	Highest Occupied Molecular Orbital
LUMO	Lowest Unoccupied Molecular Orbital
$g(E_f)$	Density of Electronic States at the Fermi Level
LSPR	Localized Surface Plasmon Resonance
BSM	Brust-Schiffrin Method
PTC	Phase Transfer Catalyst
TOAB	Tetra-N Octylammonium Bromide
DCM	Dichloromethane
TEM	Transmission Electron Microscopy
ICP-AES	Inductively Coupled Plasma Atomic Emission Spectroscopy
NMR	Nuclear Magnetic Resonance
CESR	Conduction Electron Spin Resonance

Acknowledgements

Throughout my time at Penn State, I have enjoyed the support and mentorship of many people. In particular, my parents have always shown unwavering support for whichever path I have chosen. This freedom ultimately allowed me to pursue chemistry and write this thesis. Among the members of the Lear group, I would like to specifically thank Ben Kaercher and Kristen Aviles, my graduate student mentors. From them, I have learned a great deal of science and technique, and I have also made great friends in the field.

I would like to say a special thank you to my PI Ben Lear for his mentorship. Ben has inspired me to pursue chemistry as a career, and in retrospect, I couldn't be more happy with my decision.

I also thank the Pennsylvania State University and support from the NSF award CHE-500000024636 for funding. The findings and conclusions of this thesis do not necessarily reflect the views of the funding agencies.

Chapter 1

Modifying Nanoparticle Electronics through Surface Chemistry

1.1 Introduction

Metallic nanoparticles have a wide range of applications in optics, catalysis, medicine, and other fields.[1] Unlike bulk materials or molecules, nanomaterials posess unique electronic and physical properties as a consequence of their size.[2] From a fundamental chemistry perspective, understanding the electronic behavior of materials is crucial as it dictates their physical and chemical characteristics. The distinct electronic properties of nanoparticles enable a wide array of behaviors not observed in bulk materials. A key objective in the development of nanochemistry is establishing control over these electronic properties to enable tailored applications of nanomaterials. To date, a large portion of existing research on nanoparticle electronic properties has focused on the role of size and shape effects.[3–5] However, other factors are also anticipated to exert electronic influence over nanomaterials. Notably, surface chemistry is expected to play a significant role due to the high surface area to volume ratio of nanoparticles. This introductory chapter covers the basic electronic structure of metals based on band theory, followed by an exploration of the tunable aspects of nanoparticles that empower chemists to manipulate their electronic properties. Finally, a brief overview of the content of this thesis is presented.

1.2 The Electronic Structure of Metallic Nanoparticles

1.2.1 The Band Structure of Metals

The electronic structure of solid systems is commonly modeled via band theory.[6] The basis of band theory comes from the molecular orbital (MO) theory for chemical bonding. In MO theory, the molecular electronic wavefunction is generated as a linear combination of the component atomic electron wavefunctions. The simplest molecular orbitals can be conceptualized by examining the dihydrogen system.[7] Each hydrogen atom, in its ground state, harbors a single electron within a 1s electronic orbital. Upon combining the two 1s orbitals, bonding and

antibonding orbitals are formed depending on the relative phases of the atomic orbitals.

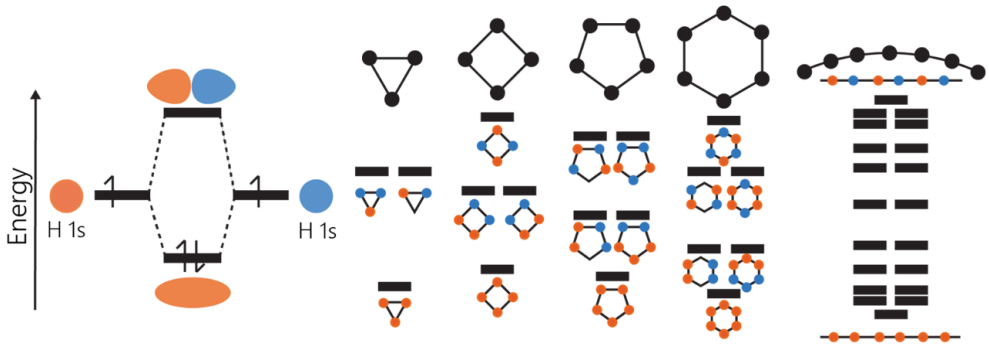

Figure 1.1: Diagram of the band structure development for Hydrogen. Blue and orange colored orbitals represent separate orbital phases. As N increases, particular geometric configurations of positive and negative phases generate degenerate MOs.
[8]

As an increasing number of component atomic orbitals are considered, the count of stabilized (bonding) and destabilized (antibonding) orbitals increases. Additionally, particular configurations of component orbitals generate degenerate (same energy) MOs. In systems with many atoms, the number of MOs becomes so great that the gap in energy between orbitals approaches zero. This results in an electronic structure characterized by a continuum of electronic energy states between the maximum and minimum energies. Upon attaining this continuum of energetic states, the structure is called a 'band'. The band is named after the atomic orbitals that are combined to form it. For instance, in the hydrogen system (depicted in Figure 1.1), the 1s band arises from the overlap of 1s orbitals. Within a band, the number of MOs at a each energy exhibits a Gaussian distribution when plotted with respect to energy. The Gaussian shape results from to the greater degeneracies (larger numbers) of MOs at intermediate energies within the band.[6] In systems with higher valence atomic configurations, we must consider multiple bands and their overlaps. A diagram of the valence band structure of gold, relevant to this work, is depicted in Figure 1.2.

The next step in developing the band structure of a material is considering the occupation of bands by electrons. Analogous to the dihydrogen model, electrons populate the available molecular orbitals from the bottom up (in the ground state). The individual atomic electron configurations and the size of the subshell provide insights into how the band will be populated. For instance, hydrogen has a $1s^1$ configuration, and the 1s subshell is capable of accommodating two electrons. Therefore, in solid hydrogen, the 1s band would be half-filled. Conversely, in the case of a more complex atom like Au ($5d^{10}6s^1$), the 5d band would be completely filled, and the 6s band would be half-filled.

The filling of the band by electrons introduces an important parameter for the behavior of materials. Specifically, the energy gap between highest occupied molecular orbital (HOMO) and lowest unoccupied molecular orbital (LUMO). If a band is completely filled, then the next available electronic state occurs at the start of the next band. Since bands do not always overlap, an energy

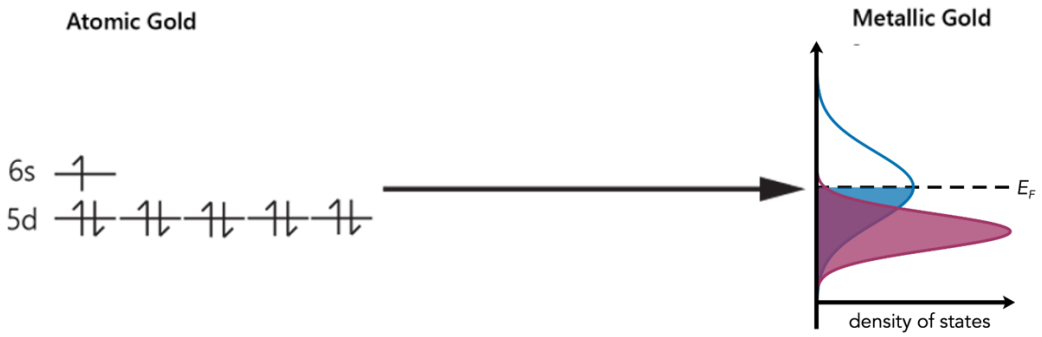

Figure 1.2: Diagram of the valence band structure of metallic gold. Bands are formed by the overlap of 5d and 6s orbitals, respectively. The density of states for each band assumes a Gaussian distribution with respect to energy. The 5d band intersects with the lower energy half of the 6s band. Filling of the band by electrons results in a fully filled 5d band and a half filled 6s band.

gap may exist between the end of one band and the beginning of the next. In metallic systems, bands are partially filled. Partial filling of the band structure results in the HOMO-LUMO gap effectively approaching zero. This is because adjacent energy levels within the band structure have no energy gap between them.[6] Consequently, due to the absence of a 'band gap', when thermal energy is supplied, electrons in metals can readily move around by promoting to higher energy states. The free movement of electrons is what characterizes a conductor.

The final critical aspect that is relevant to this study is how the ground state is characterized for metallic systems. In band theory, the ground state energy of the system is delineated by the Fermi level. The Fermi level is defined as the energy level at which, under thermodynamic equilibrium, there exists a 50% probability of electron occupation.[9] At absolute zero temperature (no thermal energy), the band structure is filled strictly from the bottom up; therefore, the Fermi level is the same as the energy of the HOMO. However, the introduction of thermal energy permits electrons in the highest occupied orbitals to freely transition to higher energy states. Consequently, the Fermi level must be defined probabilistically. By its definition, the Fermi level can be conceptualized as the energy level which, given a specific temperature (i.e., thermal energy), you are highly likely to actually find an electron. Although electrons may occupy higher energy states due to thermal fluctuations, if you look at those energy states at a given moment in time, then the chance of finding an electron is low.[9] Thus, the Fermi level for a solid serves as an indicator of the system's ground state energy.

1.2.2 Density of Electronic States at the Fermi Level

As mentioned in the previous section, energy levels within the band structure are home to varying numbers of molecular orbitals depending on the degeneracy. We can refer to the number of molecular orbitals (also including electron spin states) around a given energy level as the 'density of electronic states'. We express the density of states at an energy level as the number of states per unit energy per unit volume of the system ($J^{-1}m^{-3}$). For the ground state of the system,

the relevant parameter is the density of electronic states at the Fermi level ($g(E_f)$). In solid-state chemistry and physics, $g(E_f)$ is a crucial parameter for describing metallic systems.[6,9] Since $g(E_f)$ conveys information about the electronic population of the ground state energy level, it is therefore related to macroscopic properties reliant on energy transfer or electronic interaction with other species. For instance, $g(E_f)$ is related to properties such as electrical and thermal conductivity, optical characteristics, and catalytic activity.[6,9] These properties and other all are of significant interest in solid-state chemistry and physics.[6,9]

1.3 Tunability of Nanoparticles

1.3.1 Size

Size effects are one of the most extensively studied domains in nanoscience.[3,5] Changes in size impact the surface area to volume ratio and the confinement of electrons within the material. At small sizes, these size effects become highly significant to the characteristics of materials.[2] For characterizing electronic properties, one of the most widely used probes in the chemical literature is the localized surface plasmon resonance (LSPR).[10] LSPR results from the oscillation of surface conduction electrons in response to irradiation by light with a wavelength exceeding the particle diameter. Upon interaction with light, electrons near the surface are displaced because of the appliaction of an electric field. This displacement results in oscillations of the particle's electron cloud in response to the oscillating electric field of the incident light-wave. LSPR manifests as a peak in the extinction spectrum relating to the resonant frequency. For spherical particles, analytical solutions to the LSPR position and size are calculated by Mie Theory.[11] With knowledge of the size, shape, and dielectric environment, Mie Theory enables calculation of the position and width of the LSPR maximum for a given nanoparticle system.

The dependence of localized surface plasmon resonance (LSPR) on particle size has been extensively characterized, particularly in gold nanoparticle systems.[3,5] The observed dependence of the LSPR bandwidth on size involves a modification to traditional Mie Theory to incorporate the dependence of the particle dielectric on size. This modification yields a modified Mie Theory capable of accurately predicting a redshift in the LSPR maximum. Experimental confirmation of the LSPR's size dependence was provided by Link and El-Sayed for aqueous, spherical gold nanoparticles with average diameters ranging from 9 to 99 nm.[5] As anticipated, the LSPR maximum demonstrated an inverse dependence on particle radius. This results in a shift to lower energies as particle size is increased. Moreover, empirical observations revealed that the LSPR bandwidth decreased with size below 25 nm and increased with size above 25 nm. This relationship between size and bandwidth is also substantiated mathematically within the Mie equations. Specifically, as particle size approaches the incident wavelength, contributions from higher-order oscillation modes escalate due to inhomogeneous polarization by the electric field.[4,11] These radiative losses contribute to plasmon broadening.

In addition to surface area and spatial confinement effects on electronics, the number of atoms is also directly related to the electronic structure.[2] For very small nanocrystals, commonly referred to as clusters, the energy gap between adjacent energy states is not sufficiently close to zero to

enable conduction electrons. As a result, small clusters behave as electronic insulators. However, as the number of atoms increases, the band structure gradually begins to resemble that of the bulk material. This transition signifies the diminishing significance of size-induced effects on the fundamental electronic structure as the nanocrystal.

1.3.2 Shape

Another extensively explored tunable aspect of nanoparticles is their shape. Similar to size, the shape of nanomaterials impacts the surface area to volume ratio and the spatial confinement of electrons within the material. A well-documented example of shape effects in the chemical literature is evident in gold nanorods.[3,4] Gold nanorods possess distinct longitudinal and transverse axes. This results in the observation of two LSPR peaks corresponding to electron oscillations along the different axes. With an increase in aspect ratio, the longitudinal LSPR peak demonstrates a linearly dependent redshift for gold nanorods. This phenomenon underscores the significant influence of nanoparticle shape on their optical properties and highlights the tunability of such properties through controlled manipulation of nanoparticle morphology.

1.3.3 Solvent Dielectric

As previously mentioned in our discussion of size effects, Mie Theory also indicates that the dielectric environment of the nanocrystal plays a significant role in influencing the LSPR.[11] The dielectric environment surrounding the metallic core is influenced by both the solvent and ligand shell. Similar to the aspect ratio of gold nanorods, the solvent dielectric is found to be linearly related to the redshift in the LSPR.[4] However, it's important to note that ligand coordination can result in changes to the electronic behavior of the core by either donating or accepting electron density. These electronic modifications to the core also contribute to a shift in the LSPR which is predicted by Mie Theory. Therefore, both the dielectric environment and ligand coordination play pivotal roles in shaping the optical properties of metallic nanoparticles.

1.3.4 Surface Chemistry

Surface chemistry is perhaps one of the most powerful tools in nanoscience. There is a functionally infinite amount of ligands that can be coordinated to nanomaterial surfaces; therefore, surface chemistry offers a near boundless dimension for particle tunability. In the chemical literature, surface chemistry is frequently explored for tuning solubility, stability, and binding, as exemplified in applications such as chemical sensors.[12,13] In particular, the high surface area-to-volume ratio of nanomaterials allows surface modifications to exert a significantly greater influence on the core compared to bulk materials. This heightened sensitivity underscores the immense impact that surface chemistry can have on the overall properties and behavior of nanoparticles.

Broadly, ligands can be broken into two parts: a head group and a tail group. It is intuitive that modifications to the head group directly influence the electronic properties of the core since they directly interact. However, the role of the tail group has also been found to be remarkably

significant. Previous studies, such as those conducted by the Lear group, have demonstrated that subtle alterations to the ligand tail group, such as varying the chain length of alkanethiols, can induce changes to the core electronics.[14] These findings underscore the interplay between ligand structure and nanoparticle electronics.

In addition to ligand identity, surface ligand density is another fundamental parameter to nanoparticle surface chemistry. In the literature, surface ligand density is often considered in catalytic assays involving nanoparticles.[15] In many catalytic nanosystems, the core serves as the active catalytic site; hence, species must access the particle surface for catalysis to proceed. Since surface ligand density has a direct impact on diffusion near the particle surface, it is expected to have an influence on catalyst tunability. Indeed, this result is reflected in the chemical literature.[15] However, a yet unexplored question concerns the direct influence of surface ligand density on the core electronics. It is reasonable to anticipate that alterations to ligand density would affect the donation of electron density to the core by the ligand shell. These modifications to the core electronics may carry significant implications on properties such as catalytic activity.[16] The exploration of this relationship serves as the motivation for this thesis.

1.4 An Outline of this Thesis

In this thesis, my focus revolves around exploring the relationship between alkanethiol surface ligand density and the electronic structure of gold nanoparticles (AuNPs).

Chapter 2 will present a synthetic methodology devised to produce thiol-protected AuNPs of varying surface ligand densities while ensuring a constant core size and morphology. This synthetic approach is established based on existing literature and a comprehensive mechanistic understanding of AuNP synthesis.

In Chapter 3, I explain the theory and procedure of experiments I performed to probe the relationship between surface ligand density and the density of states at level. Through these results, I aim to elucidate how varying surface ligand densities influence the electronic properties of AuNPs.

Finally, Chapter 4 will serve as a culmination of my findings, summarizing our current understanding of the relationship between surface ligand density and electronic properties of AuNP systems. Additionally, I present potential avenues for future research, highlighting areas of interest and directions for further experimentation.

Chapter 2

Establishing Independent Synthetic Control over Core Size and Surface Ligand Density for Thiol-Protected AuNPs

2.1 Introduction

Thiol-protected gold nanoparticle (AuNP) systems have been a large part of nanoparticle research for over three decades. Compared to other AuNP systems, thiol-protected AuNPs posess several advantageous qualities such as facile synthesis, stability, and solubility in a broad range of organic solvents.[13,17–19] These properties have led to their widespread use and exploration in various fields. For surface chemistry investigations, thiols offer adjustable functionality and allow for relatively high achievable ligand surface densities.[13,18–21] Previous studies, including work by the Lear group, have investigated the influence of alkane chain length on the electronic structure of nanoparticles using alkanethiol-protected AuNP systems.[14] Building upon this foundation, this work aims to further our understanding of these systems. Specifically I will be focusing on the role of surface ligand density in alkanethiol-protected AuNPs while maintaining a constant core size and morphology. To achieve this objective, I propose a modified synthetic method derived from existing chemical literature. The modified method will enable independent control over both the core size and surface ligand density of the AuNPs. This synthetic approach will facilitate investigations into the relationship between surface ligand density and the electronic properties of AuNPs.

2.1.1 The Brust-Schiffrin Synthesis

The Brust-Schiffrin method (BSM) is a synthetic procedure for generating gold nanoparticles functionalized with alkanethiol ligands.[13] The BSM offers notable advantages compared to other AuNP syntheses, as it can be performed at room temperature in a one-pot synthesis setup. One of the hallmark features of the BSM is its capability to generate small AuNPs with typical average batch sizes between 2 to 3 nm in diameter.[13,22,23] The BSM has been extensively utilized in the chemical literature, thereby solidifying its reputation as a versatile and efficient approach for the

synthesis of small gold nanoparticles.

A general overview of the BS method is as follows: (1) Transfer of gold ions to organic phase: An aqueous solution of chloroauric acid ($HAuCl_4$) is added to an organic phase containing a phase transfer catalyst (PTC). The PTC is a surfactant molecule. Typically, the quaternary ammonium salt tetra-N octylammonium bromide (TOAB) is used. TOAB facilitates the transfer of gold ions into the organic phase. Visual confirmation of gold ion transfer is confirmed by a change in color from colorless to orange-red in the organic phase. (2) Addition of thiol ligand: The now colorless aqueous phase is discarded, and the desired alkanethiol ligand is introduced into the organic phase. The solution is then stirred for a certain period to ensure thorough mixing. (3) Formation of gold nanoparticles: An aqueous solution of a reducing agent, typically sodium borohydride ($NaBH_4$), is added to the stirring organic phase solution. Rapid reduction of gold ions to Au(0) leads to the formation of AuNPs. The formation of AuNPs is characterized by a dark brown and eventually purple-black coloration in the solution. The reaction mixture is stirred for several hours to ensure complete nanoparticle formation. Excess thiol ligand is removed by washing the AuNP product with an antisolvent (e.g., ethanol or methanol) and centrifugation. The resulting black powder constitutes the final product.

The dried AuNPs exhibit excellent dispersibility in various organic solvents, including dichloromethane (DCM), toluene, tetrahydrofuran (THF), and deuterated chloroform ($CDCl_3$), among others. A schematic depicting the BSM steps in shown in Figure 2.1.

Numerous research groups have systematically explored tuning the parameters of the BSM to produce AuNPs with average sizes ranging from 1.5 to 8 nm.[13,18,22–24] Moreover, a wide array of modified BSM syntheses exist in the literature. Often, modification involves different noble metal precursors, alkyl-thiosulfate or disulfide compounds instead of thiols, or alterations to reaction parameters such as reaction time.[25–27] These modifications provide versatility and enable tailored synthesis approaches to meet specific research objectives and applications.

A notable characteristic of the BSM is the ability to tune the mean particle size as a function of the molar thiol to gold ratio employed during synthesis. As the S:Au ratio in the reaction decreases, the mean core size of the resulting gold nanoparticles is observed to increase.[22] The mechanism underlying size control through ligand to metal precursor ratio is distinct from many other wet chemical AuNP syntheses. In many other syntheses, size variation is typically tuned as a function of reducing agent concentration following the classical LaMer mechanism.[28–30]

The ligand related size dependence exhibited by the BSM has sparked significant interest in the scientific community. This has lead many research groups to investigate the underlying mechanism of the BSM. The objective of these investigations is to gain a deeper understanding of the BSM and to develop strategies for enhancing control over particle synthesis.[24,25,31–34] Figure 2.2 from Perala et al. succinctly summarizes the observed dependence of particle diameters on the molar S:Au ratio from a number of studies in the chemical literature.

Current mechanistic models of the BSM involve understanding the balance between nucleation, growth, and surface passivation.[31] Upon the addition of the reducing agent, AuNPs nucleate and grow in solution in a process that has been suggested to follow the LaMer mechanism.[13] However,

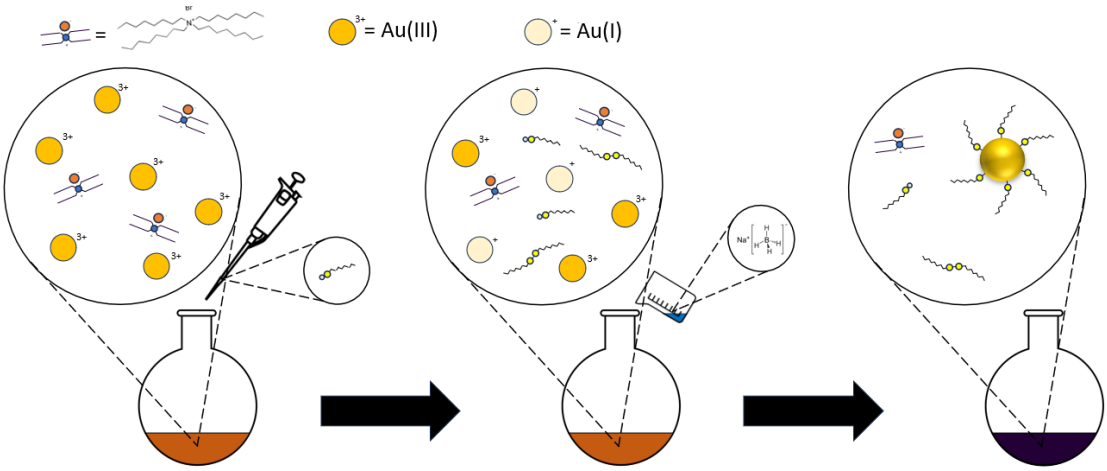

Figure 2.1: Schematic depicting the addition order involved in a standard Brust-Schiffrin Method synthesis. Au(III) ion transfer to toluene is facilitated by TOAB. Upon addition of the thiol ligand, some Au(III) is partially reduced to Au(I), and thiol ligands are concurrently oxidized to disulfides. Upon addition of $NaBH_4$, Au(III) and Au(I) ions are reduced to Au(0) which nucleate and grow into AuNPs. The AuNP surface is passivated by coordination with thiol and disulfide in solution.

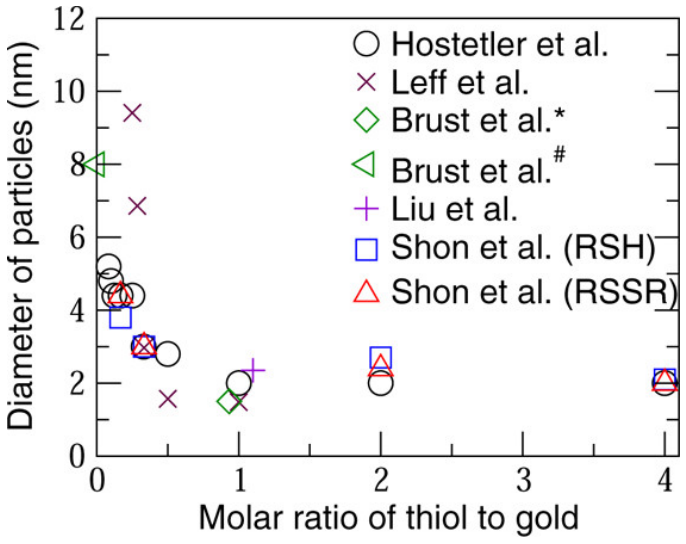

Figure 2.2: Results from the chemical literature for mean core size plotted against the molar S:Au ratio employed using the BSM. Below a molar ratio of 1:1 S:Au, the mean core diameter is observed to increase significantly.

the growth process is halted by capping with thiol ligands. The thiol ligands passivate the AuNP surface, thereby preventing further growth at that site.[32] Nonetheless, uncapped surfaces on the nanoparticle continue to grow. This leads to complex kinetic behavior.

The kinetics governing this process are also complicated by interactions between the thiol and gold ions. It is well-established that the addition of thiol ligand to the gold ion solution results in the partial reduction of Au(III). This leads to the coexistence of aqueous gold in both Au(III) and Au(I) oxidation states.[31] However, there is disagreement regarding the nature of thiol-mediated gold reduction. Brust et al. originally proposed the formation of an —$(AuSR)_n$— polymer.[13] Subsequent studies have isolated this Au(I) polymer from dried reaction mixtures and demonstrated its ability to produce thiol-protected AuNPs upon reductant addition.[23] Conversely, other studies contest the polymer formation. Another common mechanism suggested is thiol-mediated reduction of gold to form (TOA)[AuX_2] complexes.[25,34]

Despite these disagreements, BSM mechanistic studies agree on the presence of Au(III) and Au(I) in solution prior to $NaBH_4$ addition. Moreover, the presence of disulfide species from oxidized thiols further complicates the kinetic parameters. Disulfides are known to produce thiol-protected AuNPs in the BSM,[23] yet the kinetic differences between thiol and disulfide capping have not been thoroughly explored. The relative ratios of Au(III)/Au(I) and thiol/disulfide contribute to a complex set of kinetic parameters believed to influence the mean particle size in the BSM.[31]

These mechanistic insights into the BSM suggest potential challenges in synthesizing separate sets of AuNPs with constant core sizes and varying surface ligand densities. The straightforward approach — adding more or less thiol ligands to the reaction — would simultaneously vary both core size and surface density as evidenced by the chemical literature. It may be possible to attempt a post-synthetic modification or ligand exchange whereby surface ligand density is altered. However, the requirement of post-synthetic processing would remove many of the favorable, facile aspects of the BSM. Therefore, in order to generate AuNPs suitable for my electronic investigations, I elected to test a modified version of the BSM.

2.1.2 ”Reversed Thiosulfate Addition Synthesis”

My synthetic procedure is originally inspired by the work of Vargas et al.[15] In their study, they explored the catalytic activity of alkanethiol capped palladium nanoparticles (PdNPs). Specifically, they explored the relationship between surface ligand density and the kinetics/selectivity of PdNP catalyzed reactions.

The synthesis of PdNPs in their study was accomplished through a modified BSM. Initially, used the same addition order as the standard BSM, but they substituted K_2PdCl_4 and alkylthiosulfate salts for $HAuCl_4$ and alkanethiols. Thiosulfates, akin to alkanethiols, exhibit similar behavior by partially reducing gold to Au(I), passivating the nanoparticle surface, and ultimately yielding thiol-protected AuNPs. However, thiosulfate-based syntheses typically result in larger average particle sizes and lower surface ligand densities compared to thiol-based syntheses. This difference is often attributed to the bulky and ionic nature of the thiosulfate head group. This is thought to lead to slower passivation kinetics and reduced maximum surface

loadings.[26]

Upon application of the initial method described above, it was observed that surface ligand density could be adjusted by varying the ligand concentration during synthesis.[35] However, similar to the original BSM, altering the ligand to metal precursor ratio also resulted in changes to the core size. Altering the core size inherently impacts the surface area-to-volume ratio which changes the total surface area in solution. Since changing the overall available catalyst surface area would interfere with their intended studies, a new synthetic route was necessary to achieve control over surface ligand density while ensuring constant core size and morphology.

In response to these findings, Vargas and colleagues proposed a ”reversed thiosulfate addition synthesis” approach. The the reversed addition approach, the reducing agent would be introduced before the ligand. Based on the mechanistic insights provided by the chemical literature, they hypothesized that the reversed addition order would enable the establishment of NP size through temporary passivation by TOAB and borohydride species.[15]

While purely TOAB-stabilized particles have been documented in the chemical literature, they exhibit limited stability over time.[36] When thiosulfate ligands are added, they outcompete TOAB at the nanoparticle surface due to the stability of the Au-S bond.[34] This leads to the formation of thiol-protected AuNPs. Since the kinetics of nucleation, growth, and passivation are governed by TOAB and sodium borohydride, the size and morphology of the nanoparticle core are established independently of the amount of ligand added.

Further experiments were performed to explore the influences of various reaction parameters. They observed that a temporary delay of 5 minutes instead of 10 seconds prior to ligand addition resulted in narrower size distributions. The observed effect was attributed to allowing more time for nucleation, growth, and temporary passivation by TOAB at a stable size. Conversely, the shorter delay led to the formation of more polydisperse particles and less consistency in the average particle size across different batches.

Desirably, they discovered that the core size remained constant as intended. The size range observed was 0.3 nm between the largest and smallest batches. Furthermore, adjusting the S:Pd ratio added during synthesis from 0.5:1 to 4:1 resulted in changing the ligand:surface-Pd ratio from 0.35:1 to 0.84:1. These findings underscored the robustness and reproducibility of their synthetic approach in achieving a decoupling of core size from surface ligand density.

A similar “reversed addition” synthesis for thiol-protected AuNPs was also completed by Li et al. during their studies of the BSM mechanism.[34] Based on H-NMR measurements, Li and colleagues hypothesized that nanoparticles were formed and temporarily encapsulated in ‘TOAX micelles’ (where X stands for Cl^- or Cl^-). Functionally, the micelle based mechanism acts in the same manner as surface capping. Based on this mechanistic insight, they successfully conducted a “reversed synthetic route” synthesis wherein the thiol ligand was added after the reducing agent. Upon implementation, they observed that increasing the stirring time from 10 minutes to 24 hours prior to ligand addition resulted in larger average core sizes. They attributed this increase to the additional time for TOAX-encapsulated particles to collide and coalesce.

2.1.3 Applying the Reversed Addition Order to the Brust Schiffrin Synthesis

Inspired by the works of Vargas and Li, I propose that alterations to the molar ligand to gold ratio in a ”reversed addition” BSM will result in AuNPs with constant core size and morphology but with varying surface ligand densities. This hypothesis is facilitated by the temporary passivation of the AuNP surface by TOAB prior to the addition of thiol ligands. By adjusting the molar ratio of ligand to gold in the synthesis, I anticipate varying degrees of surface coverage by thiol ligands while maintaining a constant core size and morphology. Higher ligand to gold ratios are expected to result in denser surface coverage; whereas, lower ratios are expected to result in sparser coverage. A schematic depicting the ”reverse addition” BSM steps in shown in Figure 2.3. Further details of the synthetic procedure can be found in the Appendix.

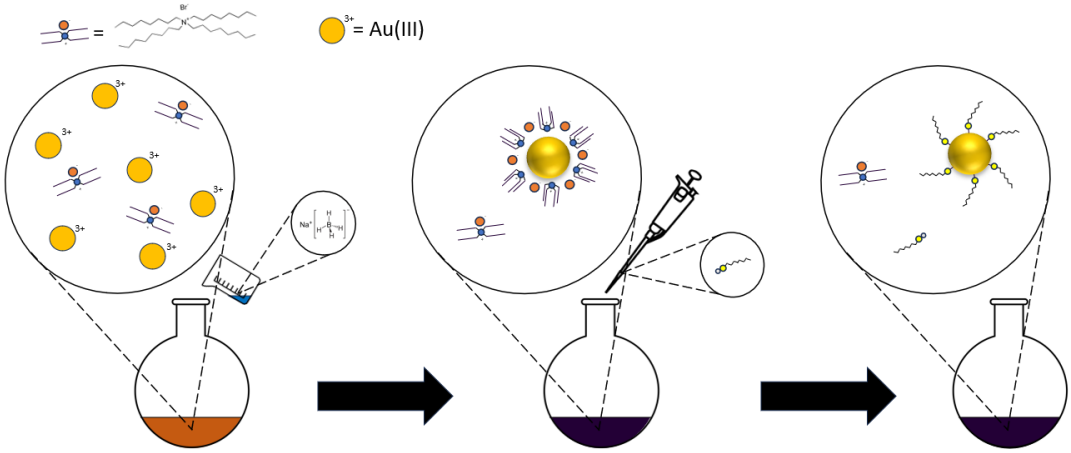

Figure 2.3: Schematic depicting the addition order involved in our reversed Brust-Schiffrin Method synthesis. Au(III) ion transfer to toluene is facilitated by TOAB. Upon addition of $NaBH_4$, Au(III) ions are reduced to Au(0) which nucleate and grow into AuNPs.The AuNP surface is temporarily passivated by coordination with TOAB in solution. Upon addition of the thiol ligand, thiols outcompete TOAB for passivation of the AuNP surface yielding thiol-protected AuNPs.

2.2 Characterization

2.2.1 Core Size

Nanoparticle core size was determined using an FEI Talos F200C Transmission Electron Microscope (TEM) from Thermo Fisher Scientific. TEM micrographs were analyzed in ImageJ, and the particle diameter was measured by the feret's diameter of the smallest circle which fully encapsulated the particle core. For each batch, a minimum of 300 particles were sized, and a histogram was plotted using plotly with the bin size determined using the Freedman-Diaconis rule. The mean core size and standard deviation were reported as the mean and standard deviation of a log normal fit of each histogram.

2.2.2 Surface Ligand Density

Surface ligand density was determined using an iCAP 7400 Inductively Coupled Plasma Atomic/Optical Emission Analyzer (ICP-AES) from Thermo Fisher Scientific. The relative ratio of gold to sulfur along with the mean core size allowed for calculation of the surface ligand density which was ultimately reported in ligands per nm^2 (see Appendix for details). The absence of free ligand molecules was confirmed by 1D ^{1}H-NMR using a Bruker Avance AV-III-HD 500 NMR Spectrometer. For ligand density calculations, particles were approximated to be spheres with a diameter corresponding to the mean core size.

2.3 Results/Discussion

2.3.1 Core Size Control

Analysis of gold nanoparticle core sizes by electron microscopy indicates that core size was successfully decoupled from the molar S:Au ratio employed during the synthetic procedure. Figure 2.1 contains a plot of the mean core diameter plotted against the S:Au ratio. TEM micrographs and histograms are available in the Appendix for reference. A linear regression analysis yields a slope of 0.0007 $\pm$ 0.014. The observed slope, within the error margin of zero, aligns well with an independent relationship between mean core diameter and S:Au ratio. Notably, an outlier value corresponding to a 3.9 nm mean core size was identified. This anomalous data point was excluded from our core size analyses; however, its significance is discussed later in this subsection.

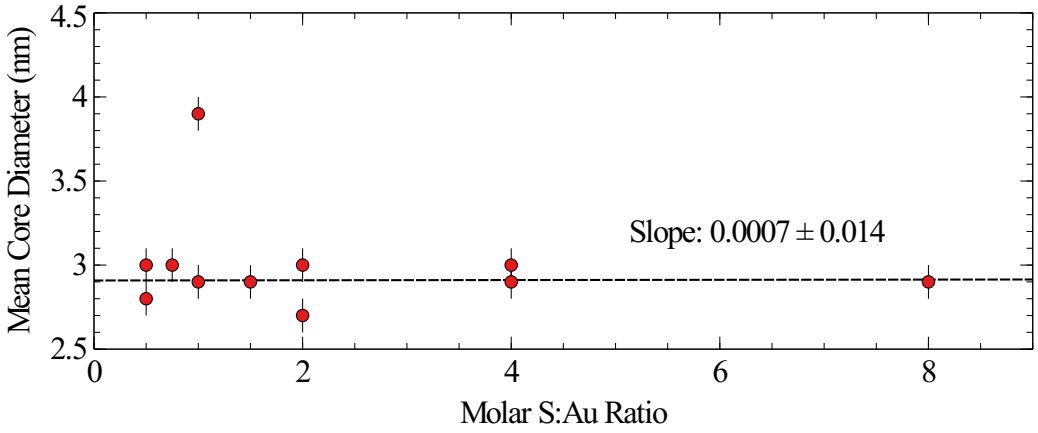

Figure 2.4: Mean core size (nm) plotted against the S:Au ratio employed during synthesis. The mean core size was determined by the mean value of a log normal fit to the core size histogram evaluated by TEM. A linear fit was generated which excludes the outlier value. The slope of our linear fit is within error of zero indicating a decoupling of the core size from the S:Au ratio.

Notably, nanoparticles synthesized with S:Au ratios less than 1:1 exhibit mean core sizes that fall within the error range of the average core size observed across all syntheses. This finding diverges from previous observations in the chemical literature, where substantial increases in

core size were noted for S:Au ratios below 1:1.[31] The fluctuations in mean core size observed across all syntheses are within 0.2 nm of the average core size. This result suggests fine synthetic control. Manual addition of reagents may have resulted in minute differences in exact masses, addition rates, and addition times between syntheses, which could account for the observed minor variations. Although such effects are typically minimal in many synthetic procedures, nanoparticle syntheses have demonstrated extreme sensitivity to synthetic conditions in previous studies.[37]

Moreover, the observed size fluctuations are not anticipated to exert a substantial influence on the electronic structure across particle batches. As previously discussed, when nanoparticles reach a sufficiently small size, the energy gap between adjacent energy levels becomes large enough that electrons cannot freely promote to higher energy states. This results in electronic behavior resembling that of an insulator.[2] However, as we will discuss in Chapter 3 of this thesis, all of our particle batches exhibit a paramagnetic effect known as Pauli paramagnetism. The observation of this paramagnetic effect requires that our particles are characterized by conduction band electrons.[38] Since all our particle batches are large enough to be characterized by a conduction band in their electronic structure, we would not expect any significant transitional behavior in the electronic band structure between particle sizes of 2.7 and 3.0 nm.

Another noteworthy aspect is the difference in the mean core size observed between the reversed addition synthesis and the standard BSM. In data compiled by Hostetler et al.,[22] the mean core diameter in relation to the S:Au ratio tends towards an asymptote at a core diameter of approximatly 2 nm. Conversely, our method yields a mean core diameter averaging 2.9 nm across syntheses. Their studies utilized identical ratios of TOAB:Au and $NaBH_4$:Au as this study. Therefore, the observed size increase is attributed to the reversed addition order. The larger observed core diameter aligns with our expectations based on the passivation kinetics of TOAB versus thiols. TOAB, being bulkier and forming associations via electrostatic interactions rather than the covalent Au-S bonds, is expected to exhibit slower passivation kinetics.[26,36] Additionally, due to the weaker interactions, we might anticipate that the collision of small TOAB-passivated particles would promote coalescence of the gold cores. These factors could contribute to the establishment of larger average core sizes. Upon the addition of the thiol ligand, the stronger association between the thiol and gold outcompetes TOAB at the AuNP surface.[34] Given that the mean core size does not change at low S:Au ratios, we hypothesize that the replacement of TOAB by the thiol ligand occurs rapidly, thereby cemeting the core size.

One statistical outlier was identified for a 1:1 S:Au ratio, where two syntheses were conducted. The first synthesis resulted in a mean core diameter of 2.9 nm. This result aligns with expected behavior based on other observed results. The second synthesis yielded a larger mean core diameter of 3.9 nm. From the perspective of a classical nucleation and growth scheme, the larger observed core size might suggest slower nucleation kinetics.[29] In such scenarios, particles that nucleate earlier tend to grow larger due to the abundance of monomers. Those that nucleate later are subject to dissolution via Ostwald ripening. This further contributes to the growth of larger particles. A driving force behind slower nucleation in our case is not immediately evident. Potential explanations could include under-addition of sodium borohydride or over-addition of solvent. Over addition of solvent would reduce reactant concentrations in the solution overall. Alternatively, the larger particle size could indicate slower passivation kinetics. Rapid surface

passivation can result in smaller sizes by impeding particle growth. Additionally, rapid passivation increases solution supersaturation (which increases the nucleation rate) since monomers cannot deposit on the surface of existing particles. Similarly to slower nucleation, a driving force for slowed passivation kinetics in our sample remains unclear. We note that the observed size increase is not consistent even across only 1:1 S:Au syntheses. Therefore, we conclude that this data does not suggest a systematic trend.

In addition to the mean core size, particle size dispersity also exhibited consistency across syntheses. Particle size dispersity was assessed by measuring the standard deviation of the size distribution. Figure 2.2 contains a plot of the standard deviation of the log normal fit to the size histograms against the molar S:Au ratio employed during synthesis. Two outlier values, indicating tighter size distributions (i.e., smaller standard deviations), were observed: the first outlier occurred for the anomalously large batch synthesized with a 1:1 S:Au ratio. Given the anomalous behavior of this batch, the outlier value for the size distribution is not significantly emphasized. The second outlier was observed for a batch synthesized with a 2:1 S:Au ratio. The mechanism underlying the tighter size distribution is not entirely clear. I hypothesize that it may be attributed to a more rapid injection of the sodium borohydride solution. Rapid nucleation events tend to favor more uniform sizes.[29]

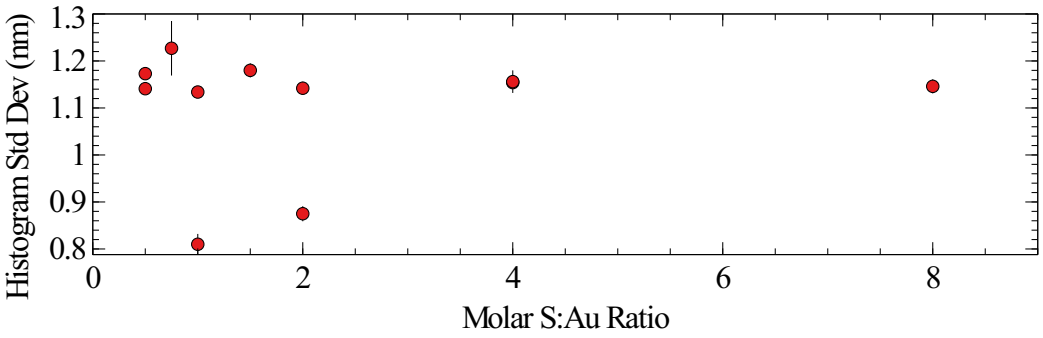

Figure 2.5: Standard deviation of mean core size (nm) plotted against the S:Au ratio employed during synthesis. The standard deviation was determined by the standard deviation of a log normal fit to the core size histogram evaluated by TEM. The standard deviation is not observed to change with S:Au. Two outliers are noted. We employ the standard deviation as a proxy for monodispersity.

2.3.2 Dependence of Surface Ligand Density on S:Au Ratio

Surface ligand density was determined by the ratio of ligands to gold (Lig:Au) in the final product measured by ICP-AES. In our calculations, we assumed the gold core to be a sphere with a diameter equivalent to the mean core size. Figure 2.3 contains a plot of surface ligand density vs the synthetic S:Au ratio. A logistic fit derived from our data suggests a maximum surface ligand density of 10.8 ± 0.3 ligands per nm^2.

The outlier 1:1 S:Au particle batch which was discussed in the previous section was excluded from the logistic fitting process. Despite not presenting as a significant outlier upon initial

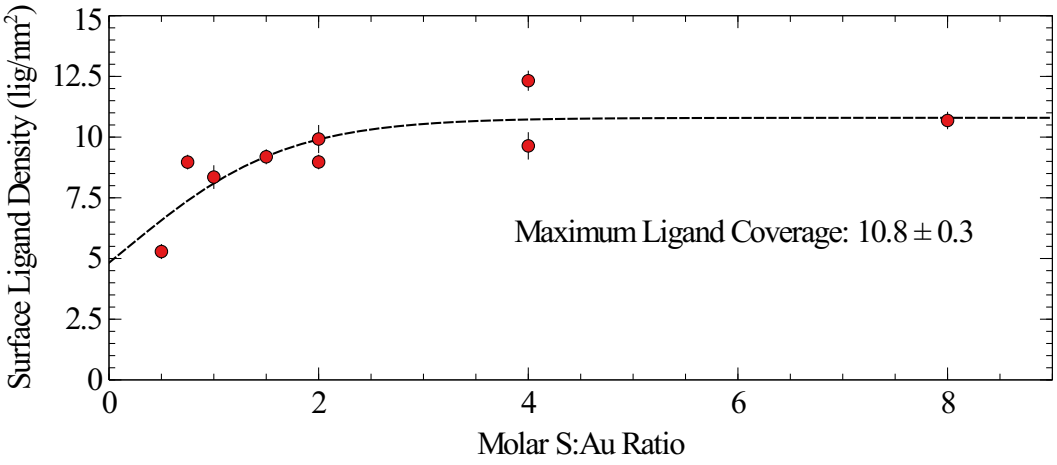

Figure 2.6: Surface ligand density (lig/nm^2) plotted against the S:Au ratio employed during synthesis. The surface ligand density was evaluated by ICP-AES in combination with our mean core size data from TEM. A logistic fit was generated excluding the size outlier batch. The maximum value of the logistic fit indicates that the maximum surface ligand density for 2.9 nm mean core size AuNPs is 10.8 $\pm$ 0.3 lig/nm^2.

examination, we anticipate that size effects influence the relationship between surface ligand density and the S:Au ratio added during synthesis. The anticipated size-dependent relationship arises from the scaling relationship between volume and surface area. If the average size of the AuNPs is larger upon the introduction of thiol ligands, there will be less total surface area per thiol ligand added. Consequently, an increase in thiol per unit surface area would be anticipated to lead to a higher surface density at the same S:Au ratio. Indeed, the observed surface density for the 3.9 nm 1:1 S:Au nanoparticle batch, measured at 10.5 ligands per nm^2, exceeds the 8.3 ligands per nm^2 observed for the 2.9 nm batch. This size-dependent effect is also evident in the relationship between the Lig:Au ratio in the final product and the surface density. Figure 2.7 displays a plot of surface density versus the molar Lig:Au ratio for the final product. From this plot, it is evident that the surface density follows a linear trend with respect to Lig:Au for particle batches with mean core diameters ranging from 2.7 to 3.0 nm. The outlier in the plot corresponds to the anomalously large batch. This aligns with our expectation that a higher surface density will be observed at the same Lig:Au ratio if the size is increased.

To ensure the accuracy of our surface ligand density measurement by ICP-AES, it was essential to verify the absence of free ligands in our final product. Since the ICP data solely provides a ratio of total S to total Au in the sample, any free ligands not contributing to the actual surface density could potentially affect the ICP results. To address this concern, we turned to 1D H-NMR data analysis. Specifically, we sought to identify the absence of a signal corresponding to the hydrogens bound to the αC of the thiol ligand. Due to the restricted motion of ligands bound to the particle surface, dipole-dipole coupling to the environment is more significant, resulting in a shorter excited state lifetime. Additionally, the effect of chemical anisotropy becomes more significant due to restricted nuclear motion. These combined effects lead to significant line broadening in the H-NMR spectrum, especially for hydrogens closest to the AuNP surface. Consequently, bound

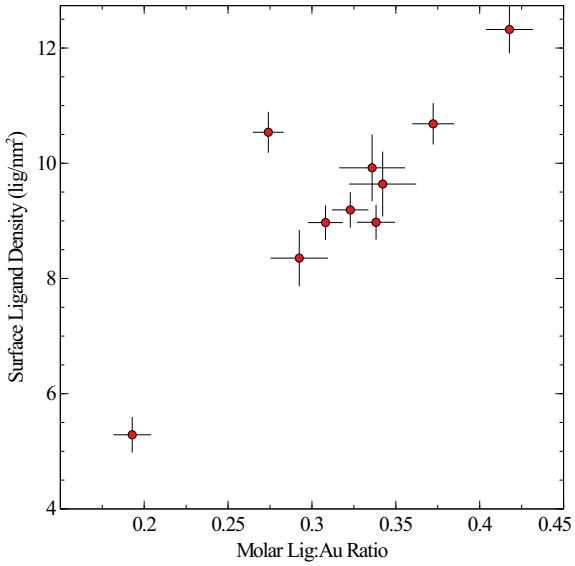

Figure 2.7: Surface ligand density (lig/nm^2) plotted against the SLig:Au ratio measured in the final product. One outlier is noted from the obsered linear trend. The points within the linear trend correspond to particle batches with mean core sizes between 2.7-3.0 nm. The outlier corresponds to a batch with a mean core size of 3.9 nm. The deviation is consistent with our expectation that changing the core size at constant reactant concentration will result in larger average surface ligand densities for the same S:Au ratio employed during synthesis.

octanethiols do not exhibit an αC hydrogen peak, whereas free ligands do. By analyzing the NMR spectra, we confirmed the absence of the αC hydrogen peak. This result indicated that free ligand concentrations were below the detection limits of our NMR instrument. An example NMR spectrum displaying the αC hydrogen peak of unbound octanethiol and the corresponding region in an NMR spectrum of purified AuNPs can be found in the Appendix. Given the low detection limits exhibited by NMR, the presence of free ligand was deemed negligible.

In the chemical literature, it is common to see surface ligand densities expressed in terms of ligands per surface atom.[15] This method of data presentation can be useful for assessing factors like fractional surface coverage and the potential of surface atoms to bond multiple ligands. However, this calculation relies heavily on assumptions regarding the precise shape of the nanoparticle core and the density of atoms on the surface. Approximating our particles to exhibit specific crystalline shapes introduces error. This is especially true for smaller particles where differences in surface area to volume ratios among different crystalline shapes become more pronounced. Additionally, we note that mass density may not be size-independent. This further complicates the calculation of ligands per surface atom. In this study, our focus is solely on comparing surface ligand densities between batches. Therefore, we prefer to report surface ligand densities in terms of ligands per nm^2. This approach requires assumptions only about the shape of the particle. We choose to approximating our particles as spheres with a diameter corresponding to the mean core size measured by TEM for simplicity.

2.4 Conclusions

Using the reversed addition order BSM, we achieved consistent core sizes while varying the octanethiol surface ligand densities of the synthesized AuNPs. Across all particle batches, the average mean core size remained at 2.9 nm, with the slope of core size relative to the S:Au ratio falling within the error margin of zero. These results indicate a dissociation between mean core size and S:Au ratio. Notably, AuNPs synthesized with S:Au ratios below 1:1 showed no discernible difference in core size. This finding diverges from literature reports on the standard BSM, where core size typically exhibits significant increases for S:Au ratios below 1:1.[31]

Based on our findings and previous studies on the BSM mechanism, we propose that core size is independently established in the reversed addition BSM through temporary passivation of the AuNP surface by TOAB. While TOAB has been documented in literature to act as a surface passivating agent for AuNPs, particles stabilized solely by TOAB exhibit long term instability.[36] Additionally, our observed mean core size of 2.9 nm exceeded the mean core sizes reported by Hostetler et al. for AuNPs synthesized with idential reagent ratios.[22] We speculate that the larger average core sizes may stem from the slower passivation kinetics of TOAB compared to alkanethiols. Slower passivation is expected to occur due to the bulky nature and ionic character of TOAB-Au interaction. Upon the introduction of alkanethiol ligands, the stronger Au-S covalent bonds cause the thiol ligands to outcompete TOAB for surface passivation. This leads to thiol-protected particles. Given the dissociation between mean core size and S:Au ratio, we infer that the ligand exchange occurs swiftly, regardless of the S:Au ratio. This rapid ligand exchange with alkanethiol ensures complete passivation of the AuNP core, thus preventing further growth.

The relationship between the S:Au ratio and surface ligand density was fit using a logistic curve. From the logistic fit, we conclude that the maximum surface ligand density for 2.9 nm mean core size AuNPs is 10.8 ± 0.3 ligands per nm^2. We also note that the maximum surface ligand density of 10.8 ligands per nm^2 corresponds to a 0.379:1 Lig:Au ratio for a 2.9 nm diameter particle. Notably, this maximum Lig:Au ratio remains beneath the minimum S:Au ratio (0.5:1) utilized in our investigation. This outcome suggests that ligand availability does not pose a limiting constraint on surface coverage.

With the particles successfully synthesized, we proceeded to the second phase of experiments outlined in this thesis: exploring the relationship between electronic properties and surface ligand density.

Chapter 3

Probing the Effects of Surface Ligand Density on Metallic Nanoparticle Electronics by Evans' Method NMR

3.1 Introduction

Electronic control is an integral aspect of chemistry. By adjusting how electrons behave in molecules and materials, chemists are able to influence the fundamental chemical and physical properties they exhibit.[6] Unfortunately, detecting alterations in the electronic properties of a material is not always straightforward. Therefore, a central aspect of electronic studies involves developing and employing methods to probe the underlying electronic properties in systems of interest. As noted in Chapter 1, the most common probe of nanoparticle electronic properties is the localized surface plasmon resonance (LSPR).[10] Because the oscillation frequency of the electron cloud depends on the properties and behavior of electrons in a material, the LSPR affords valuable information about the particle's electronics. Nonetheless, it has limitations. For instance, boundary conditions play a significant role in the LSPR position since they influence the ability of the electron cloud to oscillate. Despite the LSPR shift, changes to the boundary conditions do not necessarily indicate changes to the fundamental properties of electrons in the material. Moreover, LSPR measurements may lack the sensitivity needed to detect subtle electronic alterations. In our case, this underscores the need for alternative characterization techniques beyond traditional absorbance methods like UV-Vis spectroscopy.

Instead of the LSPR, we rely on the density of states at the Fermi level ($g(E_f)$) as a proxy for the electronic properties of small gold nanoparticles. As previously discussed, knowledge about $g(E_f)$ affords extremely valuable information about the electronics of solid-state materials.[6,9] I hypothesize that alterations to the surface ligand density will induce changes to $g(E_f)$, thereby enabling enhanced electronic control through surface chemistry.

3.1.1 Measuring the Density of Electronic States at the Fermi Level

When considering $g(E_f)$ for colloidal metallic nanoparticles, it is natural to wonder why this parameter has not been widely seen in the chemical literature. The lack of discussion regarding $g(E_f)$ can be attributed, at least in part, to challenges associated with its measurement. Techniques commonly employed by physicists and chemists to investigate $g(E_f)$ — x-ray photoelectron spectroscopy, angle-resolved photoemission spectroscopy, and x-ray magnetic circular dichroism — require high vacuum conditions. This is unsuitable for colloidal systems of interest. As a result, probing $g(E_f)$ for colloidal systems requires alternative approaches. Previous work by the Lear group has proposed a method to measure a related parameter directly linked to $g(E_f)$: Pauli paramagnetism.[39]

3.1.2 Pauli Paramagnetism

Pauli paramagnetism (χ^{Pauli}) is a phenomenon that occurs in metallic systems. χ^{Pauli} is related to $g(E_f)$ by the following relation:

$$\chi^{Pauli} = \mu_0 \mu_B^2 g(E_f)$$

where μ_0 is the permitivity of free space and μ_B is the Bohr magneton.[38] By this relation, knowledge of χ^{Pauli} facilitates calculation of $g(E_f)$.

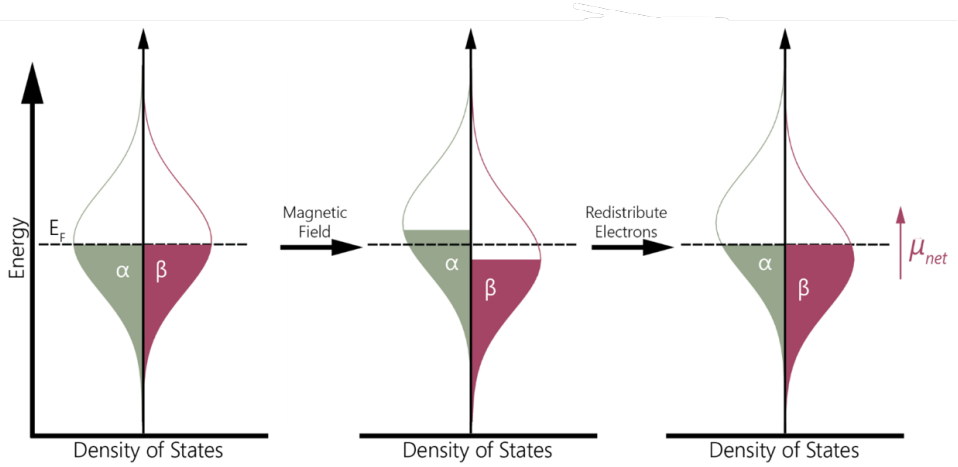

Figure 3.1: Diagram of how pauli paramagnetism arises in systems with conduction electrons. Upon the application of an external magnetic field, zeeman splitting of the α and β spin manifolds is induced. Following splitting, electrons from the destabilized manifold move to the available stabilized orbitals to maintain a constant Fermi level. The movement of electrons generates a net magnetic moment on the material. The strength of magnetic moment induced in response to an external field is known as the pauli paramagnetic susceptibility (χ^{Pauli}).

χ^{Pauli} results from the partial filling of valence bands that is characteristic of metallic systems. In these systems, each occupied electronic orbital accommodates both α and β spin state electrons. Therefore, the band structure can be divided into two spin manifolds. In the absence of an

external magnetic field, these spin manifolds are degenerate and are therefore equally populated. As a result, bulk gold is diamagnetic. Tthe application of an external magnetic field induces Zeeman splitting of the α and β spin manifolds based on if they are aligned either parallel or antiparallel to the external field direction. Conventionally, the α manifold is destabilized while the β manifold is stabilized. Given that the valence band of a metallic particle is only partially filled, electrons can transition from the destabilized α manifold to the stabilized β manifold. This electron movement generates a net spin within the system which corresponds to an induced magnetic moment. Notably, the induced magnetic susceptibility is paramagnetic. Paramagnetism indicates alignment with the external magnetic field as a result of stabilization of the parallel spin state. It is necessary for the system to exhibit conductivity to facilitate electron movement into the stabilized spin manifold. Since metallic nanoparticles above a certain size are conducting, they exhibit Pauli paramagnetism.[38]

3.1.3 Probing χ^{Pauli} Through Evans' Method NMR

To quantify χ^{Pauli} of our AuNPs, we employ Evans' Method NMR as proposed by the Lear group.[39] Evans' Method NMR is primarily used to measure the magnetic susceptibility of paramagnetic solutes within a diamagnetic solvent. In this experiment, the magnetic susceptibility is determined by detecting changes in the resonant frequency of solvent molecules due to the local magnetic field of the paramagnetic species. By analyzing the shift in peak frequency and considering the parameters of the NMR instrument, we can calculate the induced magnetic moment of the sample.

Evans' Method NMR measurements typically utilize two coaxial NMR tubes. The inner tube contains the same solvent as the outer tube, but it lacks any sample. This setup allows the inner tube solvent peak to serve as a reference for the peak shift of the outer tube solvent peak. However, due to the small magnitude of χ^{Pauli} compared to isolated paramagnetism, the peak shift we intend to observe is small. This could lead to overlap between the reference and shifted peaks which would interfere with our measurement. To enhance sensitivity, we modify the standard Evans' Method procedure. In our approach, the inner coaxial tube contains dichloromethane (DCM) as a reference peak, and the outer tube contains chloroform ($CHCl_3$). We conduct two separate measurements: first, a spectrum is acquired with the DCM insert and pure $CHCl_3$ in the outer tube. Then, a second spectrum is obtained with the same DCM insert and AuNPs dissolved in $CHCl_3$ in the outer tube. By observing the stationary DCM peak, we can accurately determine the shift of the $CHCl_3$ peak. Utilizing the magnitude of the peak shift and the parameters of the NMR instrument, we can calculate the observed magnetic susceptibility.

It is important to note that the observed magnetic susceptibility is not equal to χ^{Pauli}. Instead, it comprises a combination of paramagnetic and diamagnetic components:

$$\chi^{Obs} = \chi^{Pauli} + \chi^{Landau} + \chi^{Core} + \chi^{Shell} - \chi^{Solvent}$$

To isolate χ^{Pauli}, it is necessary to calculate and subtract the contributions from the other terms in the equation.

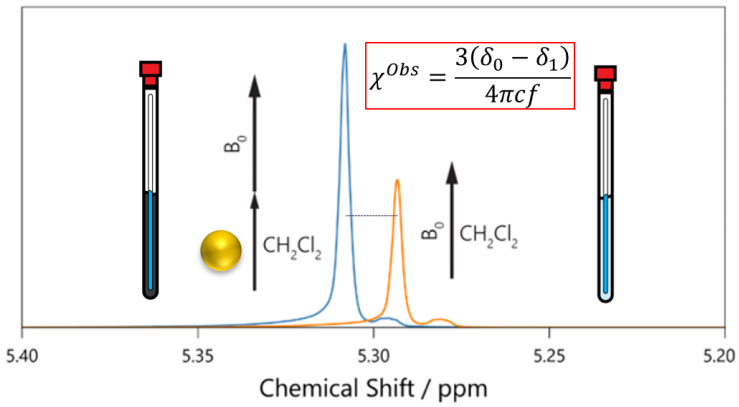

Figure 3.2: Diagram depicting how Evans' Method NMR measurements are taken. In the absence of a paramagnetic sample, solvent molecules (DCM, in this case) exhibit a particular chemical shift corresponding to the strength of the external magnetic field and the chemical environment. When a paramagnetic sample is added, the solvent molecules exhibit a different chemical shift since the net magnetic field in the sample is a combination of the external NMR magnetic field and the magnetic field generated by the paramagnetic species. The shift in the peak is measured relative to an insert of pure solvent whose position does not change. From the peak shift, the magnetic susceptibility of the sample can be calculated.

8

χ^{Landau} represents a diamagnetic component of the magnetic susceptibility, which can be understood through Lenz's law: when mobile electrons are subjected to an external magnetic field, they generate a ring current that produces a magnetic moment opposing the external field. While the classical explanation of Landau magnetism is not directly applicable to nanoscale systems, quantum mechanical orbital effects still contribute to diamagnetism referred to as χ^{Landau}.

χ^{Core} accounts for the diamagnetic contribution arising from the non-valence gold electrons in the filled core shells (1s - 5d). Similarly, χ^{Shell} accounts for the diamagnetic effects originating from the ligands. Since the ligands possess filled molecular orbitals, χ^{Shell} adds another diamagnetic component.

$\chi^{Solvent}$ represents the diamagnetic susceptibility of the solvent. As our AuNPs displace solvent molecules, the contribution of $\chi^{Solvent}$ is subtracted from the observed magnetic susceptibility.

While some research groups have reported isolated paramagnetism AuNPs, prior investigations by the Lear group indicate that it is absent in octanethiol NP systems. Their results are drawn from the relationship between temperature and the magnetic response.[39]

By utilizing our mass fraction determined through ICP-AES, we can compute the remaining terms and isolate χ^{Pauli}. Further elaboration on the calculations is provided in the Supporting Information from the paper by Litak et al. of the Lear group.[39]

It is crucial to clarify the nature of the conclusions drawn regarding $g(E_f)$ in our discussion. We do not assert that our values for $g(E_f)$ are quantitative. Due to the inherent assumptions made

in our calculations, our calculated value of $g(E_f)$ may not accurately reflect the true value for the system. Therefore, instead of firm quantitative conclusions about $g(E_f)$, our objective is to ascertain qualitative conclusions about trends and relationships between values.

3.2 Instrumentation

Evans' Method NMR Spectra were taken using a Bruker Avance AV-III-HD 500 NMR Spectrometer. NMR peaks for $CHCl_3$ and CH_2Cl_2 were fit with lorenzian curves for determination of the peak shift. The python script used to determine the Evans' Method NMR peak shifts is available online at github.com/ProfLear/EvansShiftFinder.

3.3 Results/Discussion

Evans' Method NMR measurements were taken for 10 total samples. One sample, which corresponded to a 0.5:1 S:Au synthetic ratio, decomposed prior to the preparation of our Evans' Method samples. Consequently, this batch was unfit for our electronic study.

For data presentation, I elected to plot $g(E_f)$ against Lig:Au ratio in the final product as opposed to surface ligand density in ligands per nm^2. This is primarily due to the variation in surface fraction with particle size. As particle size increases, the proportion of gold atoms comprising the surface decreases due to the scaling of volume and surface area. Consequently, the same change in surface ligand density would be expected to exert a greater impact on the electronic properties of smaller particles compared to larger ones. If all our particles were the exact same size, surface ligand density and Lig:Au ratio are proportional. While our particles do not exhibit significant size variations when considering electronic structure, there are still slight fluctuations between batches. Additionally, I hope in the future to investigate the relationship with larger particles. Therefore, I concluded that the more appropriate parameter to plot against $g(E_f)$ is the molar Lig:Au ratio.

Our results indicate that changes to Lig:Au ratio of the final product correlates with changes to the density of states at the Fermi level. A plot of $g(E_f)$ vs molar Lig:Au ratio is shown in Figure 3.1. From the data, $g(E_f)$ appears to trend downward as Lig:Au is increased.

One notable outlier in our data was observed for particles synthesized with a 0.75:1 S:Au ratio. This batch exhibited an anomalously large value for $g(E_f)$. Upon investigation, we propose that this outlier value is attributed to two main factors: poor shimming in the NMR magnet and sample decomposition over time. Achieving proper shimming in Evans' Method NMR measurements poses a consistent challenge due to the presence of coaxial NMR tubes and nanoparticles in solution. These factors can disrupt the homogeneity of the magnetic field. Inadequate shimming can distort the expected Lorenzian line shapes of NMR signals which affects our peak shift determination. Visual inspection revealed that the sample underwent decomposition. This is evidenced by the black powder product gradually turning gold over time. Given that the sample was stored for over two months and underwent multiple cycles of redispersion in solvent, it is plausible that the particles aggregated over time into bulk gold powder. Particles with lower surface ligand densities, such as those synthesized with the 0.75:1 S:Au ratio, may be less stable against

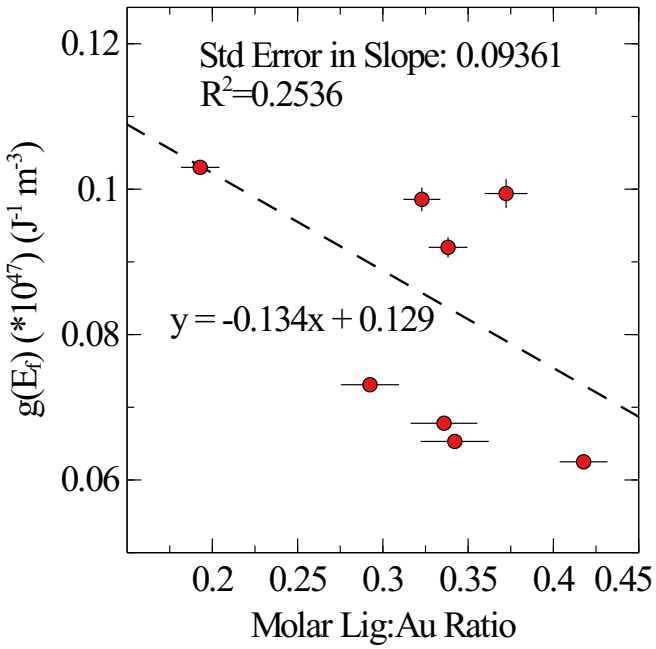

Figure 3.3: $g(E_f)$ plotted against the molar Lig:Au ratio of the sample. $g(E_f)$ exhibits a downward trend based on the available data. One outlier value is observed.

aggregation over time. Moreover, the observed color change aligns with the expected outcome of particle aggregation. Visual comparisons of fresh and decomposed samples are provided in the Appendix. Unfortunately, due to time constraints, we were unable to repeat the synthesis or conduct another Evans' Method NMR experiment for the outlier data point.

The observed relationship between $g(E_f)$ and Lig:Au suggests a coupling between Lig:Au (or equivalently, surface ligand density at a constant core size) and the electronic behavior of the gold nanoparticle core. However, the mechanism underlying this electronic tuning remains uncertain based solely on our findings. Without additional information, it is challenging to determine whether the decrease in $g(E_f)$ corresponds to the Fermi level (E_f) increasing or decreasing within the electronic band structure. Alternatively, it may indicate a change in the underlying electronic band structure due to ligand conjugation.

Drawing from chemical intuition and previous research conducted by the Lear group, I propose that the observed changes in $g(E_f)$ result from an upward shift in E_f within a band structure that closely resembles bulk gold. Thiolates, which are soft Lewis bases, are expected to bond to the AuNP surface through electron donation. Therefore, at higher surface densities, increased electron donation is expected. This would be anticipated to lead to a rise in E_f. The expected band structure resembling bulk gold, an increase in E_f corresponds to a decrease in $g(E_f)$ (See figure 1.2, 3.4).

My hypothesis is further supported by prior work from the Lear group. In a paper by Cirri et al.[14] they explored the relationship between alkanethiol chain length and $g(E_f)$. In their experiments, they observed a similar decrease in $g(E_f)$ with increasing ligand chain length. This is consistent with the anticipated shape based on a Gaussian distribution of density of states.

They also used conduction electron spin resonance (CESR) techniques to determine the electronic g-factor. The g-factor is another important electronic parameter. Their g-factor results further supported the proposed mechanism of electron donation to the core by the ligand shell. While we do not directly match our data to a Gaussian density of states distribution, we assume a similar mechanism governing the modification of $g(E_f)$ between our experiments and theirs. Thus, we infer that the thiol ligands likely drive E_f upwards. Further investigation is warranted to confirm this mechanism definitively.

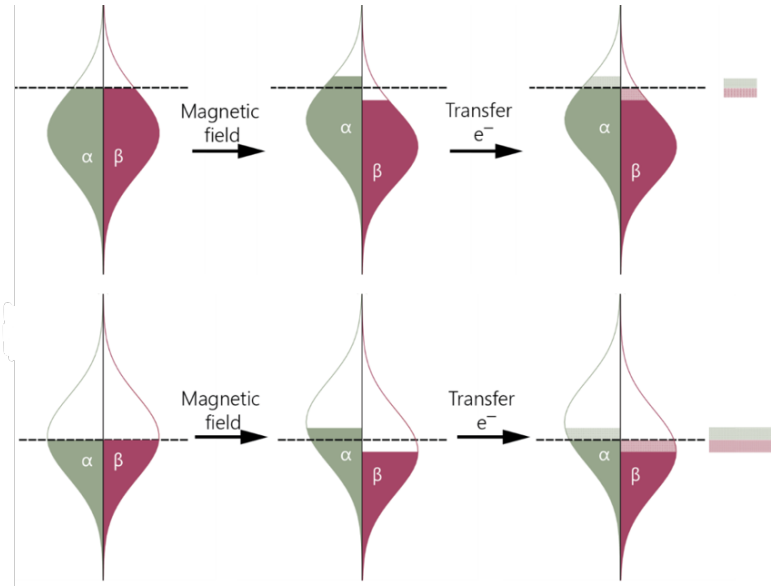

Figure 3.4: Diagram of how $g(E_f)$ affects the pauli paramagnetism. The application of an external magnetic field induces the same degree of zeeman splitting of the α and β spin manifolds. If $g(E_f)$ changes, more or less electrons will be destabilized by zeeman splitting, and therefore the strength of the magnetic moment induced will change. For a Gaussian density of state distribution, raising the Fermi level is expected to result in a weaker pauli paramagnetic susceptibility.

3.4 Conclusions

Based on our findings, we conclude that variations in surface ligand density of alkanethiols at a constant core size lead to alterations in the density of states near the Fermi level for AuNPs. Specifically, increasing surface ligand density, and consequently the Lig:Au ratio at a constant core size, results in a decrease in the density of states near the Fermi level. This observation aligns with our chemical intuition, which suggests that increased surface ligand density leads to increased electron donation by the thiolate ligand shell to the gold core. Additionally, particles with a mean core size of 3.9 nm exhibit no significant deviation from this observed trend when plotted against the Lig:Au ratio. We interpret the modifications to $g(E_f)$ in light of the Gaussian-shaped relationship anticipated for the gold 6s density of states versus energy. Accordingly, an increase in electron donation to the core corresponds with a decrease in $g(E_f)$ (See Figure 1.2, 3.4).

However, it's important to acknowledge that our dataset is limited and constitutes preliminary findings in this area. To conclusively establish the relationship between surface ligand density and electronic properties, further experiments are necessary. In particular, it would be beneficial to focus on syntheses involving S:Au ratios less than 1:1. These S:Au ratios generate the greatest variations in surface ligand density.

Chapter 4

Future Directions and Conclusions

4.1 Future Directions

4.1.1 Expansion and replication of our existing dataset

As highlighted in Chapter 3 of this thesis, our present study is based on a limited dataset. This makes it challenging to draw definitive conclusions. While we observe an apparent trend in $g(E_f)$, we cannot conclusively assert that our variables are linked in the precise manner observed here. Therefore, to strengthen our initial findings, it is imperative to replicate and extend the experiments conducted in this thesis. Specifically, I aim to synthesize more particle batches using S:Au ratios less than 1:1, as these ratios seem to display the most significant fluctuations in surface ligand density.

Furthermore, I am also interested in exploring lower S:Au ratios than those discussed in this thesis. The minimum surface ligand density observed was 5.3 ± 0.3 lig/nm^2. This surface density, for a 2.9 nm particle, corresponds to 0.19 ± 0.01 ligands per gold atom. Consequently, I am interested in if lower surface loadings are achievable and if they remain stable against decomposition. During my experiments, a batch of particles was synthesized with a 0.25:1 S:Au ratio; however, these particles are not discussed in this thesis. They were observed to decompose under dry storage after approximately 3 days. Unfortunately, I lacked sufficient time to retest these particles and gather data in a more expedited manner.

Furthermore, to bolster my findings on the electronic behavior of our particles, I would propose complement $g(E_f)$ measurements with conduction electron spin resonance (CESR) experiments. CESR measurements would allow us to determine the electronic g-factor of our particles. This g-factor, combined with data on the density of states, offers crucial insights into the electronic properties of the system. Such additional information could help refine our understanding of the mechanisms underlying the modifications observed in $g(E_f)$ within our system.

4.1.2 Size dependence on the relationship between $g(E_f)$ and surface ligand density

In light of the initial findings presented in this thesis, an additional point of interest is the possibility of size effects. As highlighted in the introductory chapter, size-dependent effects are characteristic of many properties of nanosystems. Because the surface area-to-volume ratio decreases as particle size increases, one result to be expected is that the same surface change would induce less overall electronic perturbation at a larger size. For instance, adding 100 ligands to an Au_{1000} particle would have less of an overall electronic impact than adding 100 ligands to Au_{100} particle. This consideration motivated us in Chapter 3 to plot $g(E_f)$ against Lig:Au directly as opposed to surface ligand density.

Another possibility is that the mechanism by which alkanethiol ligands interact with the core itself is size dependent. The possibility of a size dependent mechanism of ligand interaction complicates our decision to plot $g(E_f)$ against Lig:Au. For simplicity, we will consider the electronic interaction by ligands using an electrostatic model for the Au-S interaction. If the charge donation per ligand is the same regardless of core size, then plotting $g(E_f)$ against Lig:Au removes size effects. Therefore, we would expect to see the same trend in $g(E_f)$ vs Lig:Au regardless of the particle sizes considered. However, if charge donation per ligand depends on the core size, then this assumption breaks down. In this case, we might expect to observe trends in $g(E_f)$ vs Lig:Au only across particle batches of the same size. Conversely, we would get a different trend or no trend in in $g(E_f)$ vs Lig:Au when multiple batches with different sizes are plotted together. Although I do not expect the mechanism of ligand interaction to change with size, I am mindful of the uniquely important role size has in studies of nanomaterials. The answer to this question would shed further light on the mechanism by which alkanethiols affect the electronic properties of AuNPs.

Based on our hypothesized mechanism for the reverse addition BSM, a core size dependent study should be simple to conduct. Namely, the core size should be tunable by varying the synthetic conditions prior to thiol addition. We would expect that lower TOAB:Au ratios would generate larger particles due to slower passivation. With a larger core size established, we can modify the surface density by adding varying amounts of thiol ligands. Similar to our work in this thesis, we would expect the surface ligand density to be tuned by varying the S:Au ratio.

4.1.3 Solvent dependence on the relationship between $g(E_f)$ and surface ligand density

Considering that the work in this thesis utilizes colloidal systems, an additional question that arises from our results is the role of solvent dielectric and size on the observed electronic modification by surface ligand density. Previous work by the Cirri et al. of the Lear group found that the solvent plays a role in the modification of core electronic properties by alkanethiol ligands.[14] These results were based on solvent dependent changes to the electronic g-factor. The g-factor is related to the average surface potential of the gold core, and surface potential is influenced by charge donation from ligand binding. They concluded that the dielectric of the solvent mediates the degree of charge transfer to the gold core by thiol ligands.

In light of these results and the work presented in this thesis, we believe that the permeability of the ligand shell by solvent influences the mediation of charge transfer. At higher surface ligand densities, solvent penetration into the ligand shell should decrease due to sterics. If the solvent interaction is restricted by the density of the ligand shell, then we would expect that the mediation of charge transfer would likewise be impacted. Changes in charge transfer by the ligand shell would subsequently be expected to impact our measurement of $g(E_f)$.

An examination of the role of solvent dielectric and shell permeability would involve changing solvent size and dielectric and investigating the changes to electronic properties including $g(E_f)$. Based on the work by Cirri et al., CESR measurements would also be of benefit for determining this relationship. We have already established in this thesis a synthetic method for generating the necessary AuNPs for such a study. Potential parameters of consequence would be solvent size and solvent dielectric.

4.2 Conclusions

In this thesis, we have presented initial findings indicating that the surface ligand density of alkanethiol-protected AuNPs influences the density of states near the Fermi energy. Employing a modified synthetic procedure derived from the chemical literature, we produced AuNPs with consistent core sizes but varying surface ligand densities. Our synthesis method is straightforward and adaptable for future investigations involving surface ligand densities. By employing Evans' Method NMR, we analyzed the alterations in the electronic properties of the gold core. The obtained dataset reveals a downward trend in $g(E_f)$ as surface ligand density increases at constant core size. We postulate that increased thiolate surface ligand densities lead to increased electron donation to the gold core, consequently elevating E_f. Assuming a Gaussian density of states, elevations in E_f correspond to a reduction in $g(E_f)$. Our findings, coupled with previous research by the Lear group, underscore the importance of surface chemistry in modulating the electronic characteristics of metallic nanoparticles. Through the ability to tune electronic properties via surface modifications, we hope to open new, targeted applications for metallic nanoparticles.

Appendix A

Supporting Information

A.1 Experimental Methods

A.1.1 Materials

Tetraoctylammonium bromide (TOAB, 98+%) was obtained from TCI. $NaBH_4$, 99%, $HAuCl_4 \cdot 3H_2O$, 1-octanethiol (98.5+%) were obtained from Sigma-Aldrich. Solvents were obtained from Fisher Chemical. All reagents were used as received without further purification, unless otherwise indicated. Before use, all glassware was washed with aqua regia and rinsed thoroughly with DI water.

A.1.2 Standard Brust-Schiffrin Method Synthesis

$HAuCl_4 \cdot 3H_2O$ (79 mg, 0.2 mmol) was dissolved in 8 mL of DI water. The aqueous $HAuCl_4$ solution was added to a 40 mL solution of TOAB (0.274 g, 0.5 mmol) in toluene, and the two-phase mixture was vigorously stirred for ca. 10 minutes. Then, the alkanethiol ligand was added to the organic phase while stirring. After an additional 5 minutes, 4 mL of a cold, freshly prepared aqueous 0.5 M NaBH4 solution was poured into the stirring solution (ca. 5s total addition time) to produce AuNPs. The reaction was allowed to stir for 3 hours, prior to purification. To purify the particles, the dark purple-black organic phase was separated from the aqueous phase. 160 mL of methanol was added to the organic phase, and the solution was left in the fridge overnight. The next day, the AuNP product was observed to precipitate, and the clear methanol layer was decanted. The precipitate was redissolved in 8 ml toluene and split into 2 centrifuge tubes. To each centrifuge tube, an additional 40 ml of methanol was added. The product was centrifuged at 10,000 rpm for 15 minutes. Following centrifugation, the supernatant was discarded. To each tube, an additional 4 ml of toluene and 40 ml of methanol was added, and the centrifugation procedure was repeated. The resulting particles were dispersible in organic solvents.[7,13]

A.1.3 Reversed Addition BSM Synthesis

$HAuCl_4 \cdot 3H_2O$ (79 mg, 0.2 mmol) was dissolved in 8 mL of DI water. The aqueous $HAuCl_4$ solution was added to a 40 mL solution of TOAB (0.274 g, 0.5 mmol) in toluene, and the two-phase mixture was vigorously stirred for ca. 10 minutes. 4 mL of a cold, freshly prepared aqueous 0.5

M NaBH4 solution was poured into the stirring solution (ca. 5s total addition time) to produce AuNPs. After an additional 5 minutes, the alkanethiol ligand was added. The reaction was allowed to stir for 3 hours, prior to purification. To purify the particles, the dark purple-black organic phase was separated from the aqueous phase. 160 mL of methanol was added to the organic phase, and the solution was left in the fridge overnight. The next day, the AuNP product was observed to precipitate, and the clear methanol layer was decanted. The precipitate was redissolved in 8 ml toluene and split into 2 centrifuge tubes. To each centrifuge tube, an additional 40 ml of methanol was added. The product was centrifuged at 10,000 rpm for 15 minutes. Following centrifugation, the supernatant was discarded. To each tube, an additional 4 ml of toluene and 40 ml of methanol was added, and the centrifugation procedure was repeated. The resulting particles were dispersible in organic solvents.

A.2 Select Particle Characterization Data

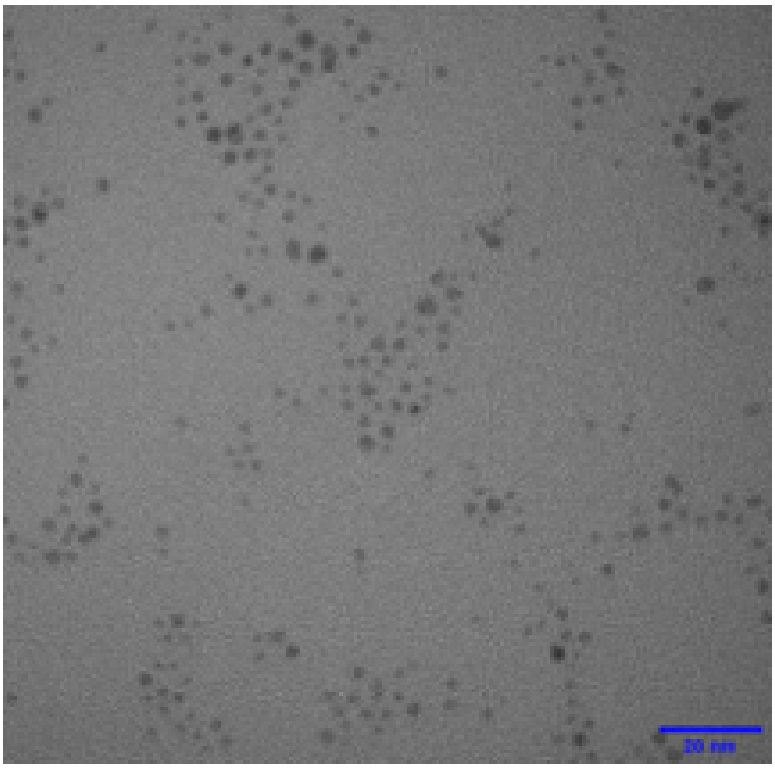

Figure A.1: TEM micrograph of AuNPs synthesized with a 0.5:1 S:Au ratio.

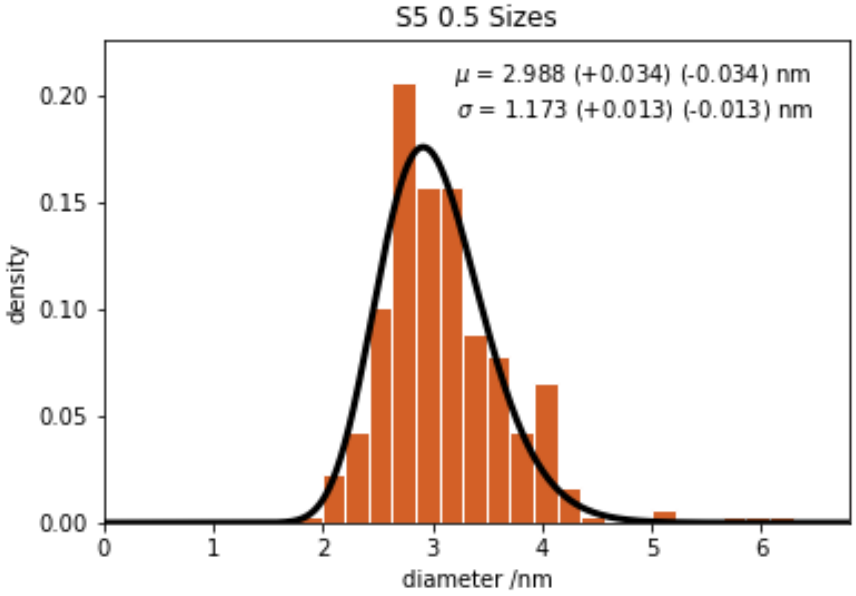

Figure A.2: Histogram and log normal fit for core sizes of AuNPs synthesized with a 0.5:1 S:Au ratio.

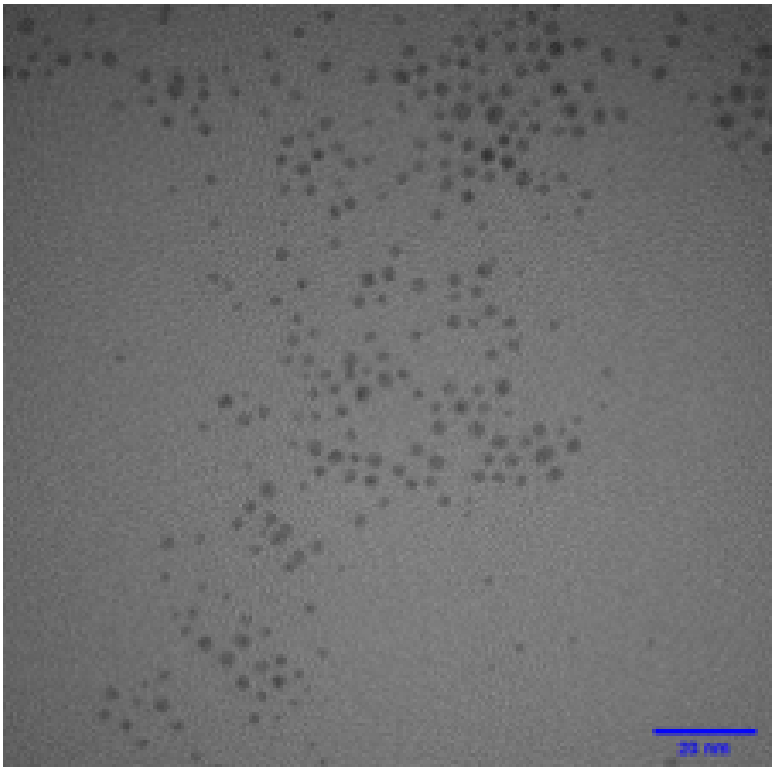

Figure A.3: TEM micrograph of AuNPs synthesized with a 8:1 S:Au ratio.

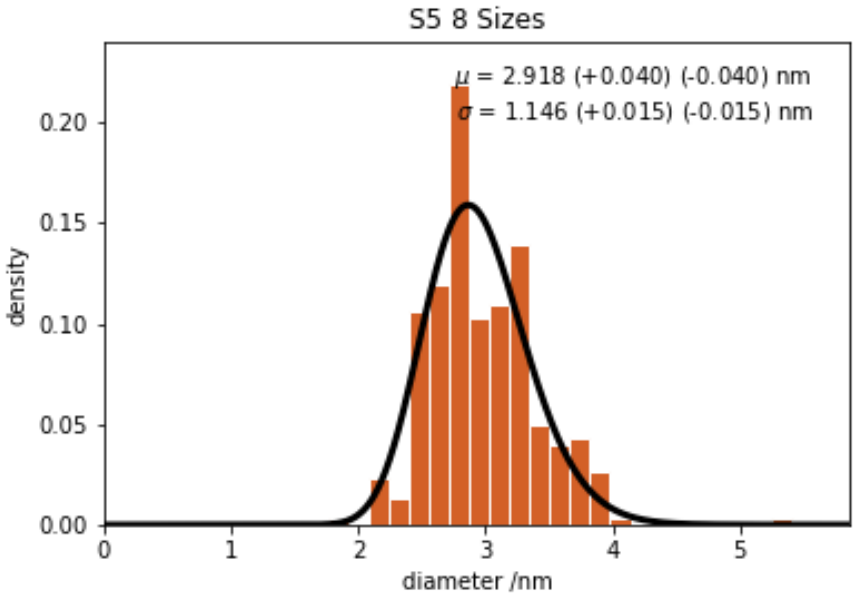

Figure A.4: Histogram and log normal fit for core sizes of AuNPs synthesized with a 0.5:1 S:Au ratio.

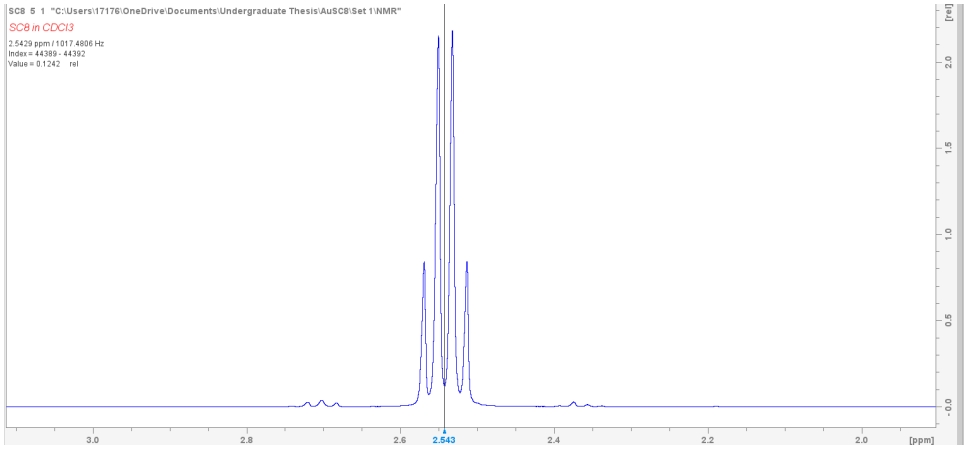

Figure A.5: Octanethiol αC peak

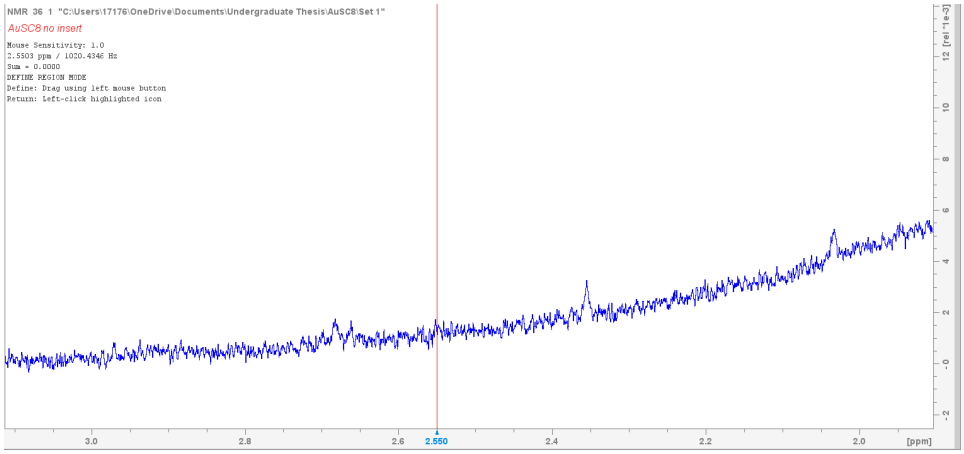

Figure A.6: Purified AuNPs exhibit no octanethiol αC peak indicating the absence of free ligands

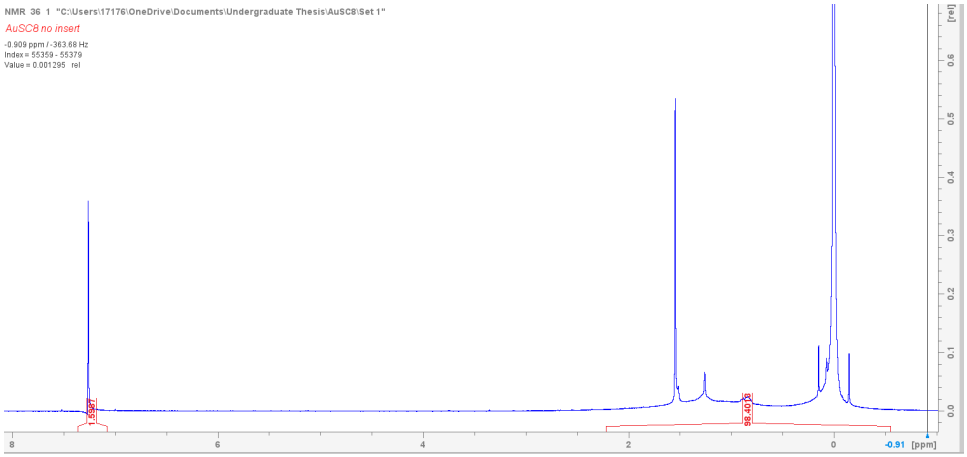

Figure A.7: Full spectrum of purified AuNPs

Figure A.8: AuNP decomposition was observed visually. The as-synthesized AuNP product appears black (right).

Bibliography

[1] V. V. Mody, R. Siwale, A. Singh, and H. R. Mody, "Introduction to metallic nanoparticles," *Journal of Pharmacy and Bioallied Sciences*, vol. 2, no. 4, pp. 267–297, 2007.

[2] E. Roduner, "Size matters: why nanomaterials are different," *Chem. Soc. Rev.*, vol. 35, pp. 583–592, 2006.

[3] V. Juvé, M. F. Cardinal, A. Lombardi, A. Crut, P. Maioli, J. Pérez-Juste, L. M. Liz-Marzán, N. Del Fatti, and F. Vallée, "Size-dependent surface plasmon resonance broadening in nonspherical nanoparticles: Single gold nanorods," *Nano Letters*, vol. 13, no. 5, pp. 2234–2240, 2013. PMID: 23611370.

[4] S. Link and M. A. El-Sayed, "Spectral properties and relaxation dynamics of surface plasmon electronic oscillations in gold and silver nanodots and nanorods," *The Journal of Physical Chemistry B*, vol. 103, no. 40, pp. 8410–8426, 1999.

[5] S. Link and M. A. El-Sayed, "Size and temperature dependence of the plasmon absorption of colloidal gold nanoparticles," *The Journal of Physical Chemistry B*, vol. 103, no. 21, pp. 4212–4217, 1999.

[6] S. L. Altmann, *Band theory of metals: the elements*. Philadelphia, PA: Elsevier, 2013.

[7] S. Cruz, *Conduction Electron Spin Resosnance of Small Metallic Nanoparticles*. PhD thesis, Pennsylvania State University, 2021.

[8] Z. Rhoden, *Surface Chemistry Characterization and Control of the Electronic Structure of Gold Nanosystems*. PhD thesis, Pennsylvania State University, 2022.

[9] A. Kahn, "Fermi level, work function and vacuum level," *Mater. Horiz.*, vol. 3, pp. 7–10, 2016.

[10] K. Willets and R. Van Duyne, "Localized surface plasmon resonance spectroscopy and sensing," *Annual review of physical chemistry*, vol. 58, pp. 282–289, 2007.

[11] G. Mie, "Beiträge zur optik trüber medien, speziell kolloidaler metallösungen," *Annalen der Physik*, vol. 330, no. 3, pp. 377–445, 1908.

[12] S. K. Kailasa, J. R. Koduru, M. L. Desai, T. J. Park, R. K. Singhal, and H. Basu, "Recent progress on surface chemistry of plasmonic metal nanoparticles for colorimetric assay of drugs in pharmaceutical and biological samples," *TrAC Trends in Analytical Chemistry*, vol. 105, pp. 106–120, 2018.

[13] M. Brust, M. Walker, D. Bethell, D. J. Schiffrin, and R. Whyman, "Synthesis of thiol-derivatised gold nanoparticles in a two-phase liquid–liquid system," *J. Chem. Soc., Chem. Commun.*, pp. 801–802, 1994.

[14] A. Cirri, A. Silakov, L. Jensen, and B. J. Lear, "Chain length and solvent control over the electronic properties of alkanethiolate-protected gold nanoparticles at the molecule-to-metal transition," *Journal of the American Chemical Society*, vol. 138, no. 49, pp. 15987–15993, 2016. PMID: 27960314.

[15] K. M. Vargas, K. A. San, and Y.-S. Shon, "Isolated effects of surface ligand density on the catalytic activity and selectivity of palladium nanoparticles," *ACS Applied Nano Materials*, vol. 2, no. 11, pp. 7188–7196, 2019.

[16] K. J. J. Mayrhofer, B. B. Blizanac, M. Arenz, V. R. Stamenkovic, P. N. Ross, and N. M. Markovic, "The impact of geometric and surface electronic properties of pt-catalysts on the particle size effect in electrocatalysis," *The Journal of Physical Chemistry B*, vol. 109, no. 30, pp. 14433–14440, 2005. PMID: 16852816.

[17] M. Giersig and P. Mulvaney, "Preparation of ordered colloid monolayers by electrophoretic deposition," *Langmuir*, vol. 9, no. 12, pp. 3408–3413, 1993.

[18] M. Brust, J. Fink, D. Bethell, D. J. Schiffrin, and C. Kiely, "Synthesis and reactions of functionalised gold nanoparticles," *J. Chem. Soc., Chem. Commun.*, pp. 1655–1656, 1995.

[19] L. Srisombat, A. C. Jamison, and T. R. Lee, "Stability: A key issue for self-assembled monolayers on gold as thin-film coatings and nanoparticle protectants," *Colloids and Surfaces A: Physicochemical and Engineering Aspects*, vol. 390, no. 1, pp. 1–19, 2011.

[20] S. R. Johnson, S. D. Evans, S. W. Mahon, and A. Ulman, "Alkanethiol molecules containing an aromatic moiety self-assembled onto gold clusters," *Langmuir*, vol. 13, no. 1, pp. 51–57, 1997.

[21] S. Chen and R. W. Murray, "Arenethiolate monolayer-protected gold clusters," *Langmuir*, vol. 15, no. 3, pp. 682–689, 1999.

[22] M. J. Hostetler, J. E. Wingate, C.-J. Zhong, J. E. Harris, R. W. Vachet, M. R. Clark, J. D. Londono, S. J. Green, J. J. Stokes, G. D. Wignall, G. L. Glish, M. D. Porter, N. D. Evans, and R. W. Murray, "Alkanethiolate gold cluster molecules with core diameters from 1.5 to 5.2 nm: Core and monolayer properties as a function of core size," *Langmuir*, vol. 14, no. 1, pp. 17–30, 1998.

[23] Y.-S. Shon, C. Mazzitelli, and R. W. Murray, "Unsymmetrical disulfides and thiol mixtures produce different mixed monolayer-protected gold clusters," *Langmuir*, vol. 17, no. 25, pp. 7735–7741, 2001.

[24] D. V. Leff, P. C. Ohara, J. R. Heath, and W. M. Gelbart, "Thermodynamic control of gold nanocrystal size: Experiment and theory," *The Journal of Physical Chemistry*, vol. 99, no. 18, pp. 7036–7041, 1995.

[25] P. J. G. Goulet and R. B. Lennox, "New insights into brust-schiffrin metal nanoparticle synthesis," *Journal of the American Chemical Society*, vol. 132, no. 28, pp. 9582–9584, 2010. PMID: 20568767.

[26] K. A. San and Y.-S. Shon, "Synthesis of alkanethiolate-capped metal nanoparticles using alkyl thiosulfate ligand precursors: A method to generate promising reagents for selective catalysis," *Nanomaterials*, vol. 8, no. 5, 2018.

[27] K. Araki, E. Mizuguchi, H. Tanaka, and T. Ogawa, "Preparation of very reactive thiol-protected gold nanoparticles: Revisiting the brust-schiffrin method," *Journal of Nanoscience and Nanotechnology*, vol. 6, no. 3, pp. 708–712, 2006.

[28] J. Turkevich, P. C. Stevenson, and J. Hillier, "A study of the nucleation and growth processes in the synthesis of colloidal gold," *Discuss. Faraday Soc.*, vol. 11, pp. 55–75, 1951.

[29] V. K. LaMer and R. H. Dinegar, "Theory, production and mechanism of formation of monodispersed hydrosols," *Journal of the American Chemical Society*, vol. 72, no. 11, pp. 4847–4854, 1950.

[30] T. Sugimoto, "Underlying mechanisms in size control of uniform nanoparticles," *Journal of Colloid and Interface Science*, vol. 309, no. 1, pp. 106–118, 2007. Matijevic Festschrift.

[31] S. R. K. Perala and S. Kumar, "On the mechanism of metal nanoparticle synthesis in the brust-schiffrin method," *Langmuir*, vol. 29, no. 31, pp. 9863–9873, 2013. PMID: 23848382.

[32] A. C. Templeton, W. P. Wuelfing, and R. W. Murray, "Monolayer-protected cluster molecules," *Accounts of Chemical Research*, vol. 33, no. 1, pp. 27–36, 2000. PMID: 10639073.

[33] R. G. Shimmin, A. B. Schoch, and P. V. Braun, "Polymer size and concentration effects on the size of gold nanoparticles capped by polymeric thiols," *Langmuir*, vol. 20, no. 13, pp. 5613–5620, 2004. PMID: 15986709.

[34] Y. Li, O. Zaluzhna, B. Xu, Y. Gao, J. M. Modest, and Y. J. Tong, "Mechanistic insights into the brust-schiffrin two-phase synthesis of organo-chalcogenate-protected metal nanoparticles," *Journal of the American Chemical Society*, vol. 133, no. 7, pp. 2092–2095, 2011. PMID: 21268580.

[35] D. J. Gavia and Y.-S. Shon, "Controlling surface ligand density and core size of alkanethiolate-capped pd nanoparticles and their effects on catalysis," *Langmuir*, vol. 28, no. 40, pp. 14502–14508, 2012. PMID: 22924990.

[36] S. R. Isaacs, E. C. Cutler, J.-S. Park, T. R. Lee, and Y.-S. Shon, "Synthesis of tetraoctylammonium-protected gold nanoparticles with improved stability," *Langmuir*, vol. 21, no. 13, pp. 5689–5692, 2005. PMID: 15952810.

[37] N. Liakakos, B. Cormary, X. Li, P. Lecante, M. Respaud, L. Maron, A. Falqui, A. Genovese, L. Vendier, S. Koïnis, B. Chaudret, and K. Soulantica, "The big impact of a small detail: Cobalt nanocrystal polymorphism as a result of precursor addition rate during stock solution preparation," *Journal of the American Chemical Society*, vol. 134, no. 43, pp. 17922–17931, 2012. PMID: 23043267.

[38] S. Blundell, *Magnetism in Condensed Matter*. Oxford University Press, 2001.

[39] N. P. Litak, L. M. Mawby, and B. J. Lear, "Surface chemistry controls the density of states in metallic nanoparticles," *ACS Nano*, vol. 16, no. 3, pp. 4479–4486, 2022. PMID: 35274922.